Generation of Fast Electrons in a CO_2 Laser Plasma Interaction

by

Grant W.J. McIntosh

B.Sc.(Hons.) University of Manitoba 1981

A THESIS SUBMITTED IN PARTIAL FULFILLMENT OF

THE REQUIREMENTS FOR THE DEGREE OF

MASTER OF SCIENCE

in

THE FACULTY OF GRADUATE STUDIES

DEPARTMENT OF PHYSICS

PLASMA PHYSICS GROUP

We accept this thesis as conforming

to the required standard

THE UNIVERSITY OF BRITISH COLUMBIA

December 1983

In presenting this thesis in partial fulfilment of the requirements for an advanced degree at the University of British Columbia, I agree that the Library shall make it freely available for reference and study. I further agree that permission for extensive copying of this thesis for scholarly purposes may be granted by the head of my department or by his or her representatives. It is understood that copying or publication of this thesis for financial gain shall not be allowed without my written permission.

Department of Physics

The University of British Columbia
1956 Main Mall
Vancouver, Canada
V6T 1Y3

Date December 15/83

ABSTRACT

Fast electrons have been observed in the $+k_L$ direction for a CO_2 laser plasma interaction. The threshold for fast electron production was found to be 10^{13} Wcm^{-2}. The number of electrons peaks and decreases for intensities greater than 6 10^{13} W cm^{-2}. Some possible theories are suggested for this behavior. When a Maxwellian fit to the electron energy distribution was used, a temperature of 121 keV was obtained. The threshold and temperature are consistent with generation by Stimulated Raman Scattering. The number of fast electrons is also shown to increase dramatically as the amount of plasma near .25 n_{cR} is increased. A computer program was also developed for the interpretation of interferograms.

TABLE OF CONTENTS

LIST OF TABLES

LIST OF FIGURES

ACKNOWLEDGEMENTS

I would like to thank my supervisor Jochen Meyer for his patience and his help in the course of my work. I would also like to thank Dr. Brian Hilko , Roman Popil and Hubert Houtman for their numerous comments and suggestions. A special thanks is extented to John Bernard for writing the plotting and ray tracing routines for the interferograms. Finally I would like to thank Richard Keeler and Al Cheuck for their invaluable technical support.

CHAPTER 1 INTRODUCTION

The study of electrons produced in laser plasma interactions is an important field of research today. Laser fusion reactors must be designed so that the so called fast electrons produced by the interactions do not inhibit the fusion process. This thesis is a presentation of experimental results on the interaction of a CO_2 laser with a gas jet target.

In laser fusion targets one wants to ablate the outer layers creating an implosion which will compress the Deuterium-Tritium fuel to high pressures at low temperatures. At these extreme conditions fusion reactions can easily occur. The ideal temperature would be near 100 keV ; practical considerations lower the temperature to 10 keV. To achieve this temperature the fuel must still be highly compressed. The best compression is obtained if the fuel is kept cold until the shock from the ablated layer reaches it. If the fuel has been warmed a much more powerful laser must be used .

Powerful lasers have pushed the frontiers of research away from the classical regions of EM - matter interactions into the non-linear regimes. New phenomena have been predicted and discovered. Some of these phenomena have serious implications for laser fusion schemes. In particular two detrimental effects can occur : electrons of very high energy can be generated and laser light can be scattered away from the target. These effects occur in the underdense blow-off plasma of the target. These high energy electrons (also called suprathermal, fast or hot electrons) can preheat the cold fuel leading to reduced

compression. The scattered laser light does not interact with the ablating layer and therefore contributes nothing to the ablation pressure which is to compress the fuel.

The objective of this thesis is to study these fast electrons identifying their origin , the number generated , and their energy distribution. In chapter 2 a summary of the theories which predict fast electrons will be presented with emphasis on Stimulated Raman Scattering and the two plasmon decay instability. Chapter 3 will outline the apparatus used to produce and detect fast electrons. The results and some minor discussion of the electron search will be expounded in chapter 4. In chapter 5 the results of an analysis of interferograms will be discussed. The results of chapters 4 and 5 will be jointly discussed and the conclusions will be reviewed in chapter 6.

CHAPTER 2 THEORY

Fast electrons can be generated by quite a number of processes. . For this thesis the parametric processes are the most important.

Parametric Processes

Parametric processes have been predicted for a number of years. Indeed Lord Rayleigh did the initial calculations in the late 19th century. There are four types of parametric decay instabilities of interest to plasma physicists. In each case , an incident electromagnetic wave (EM wave) decays into two other waves , subject to the conditions of conservation of frequency and conservation of wave vector. The waves must also obey the appropriate dispersion relations. In the parametric instability the decay products are an ion acoustic wave (IA) and an electron plasma wave (EPW). In Stimulated Brillouin Scattering (SBS) the decay products are an IA wave and a scattered EM wave. In two plasmon decay the decay products are two EPWs. In Stimulated Raman Scattering(SRS) the decay products are an EPW and a scattered EM wave. The theory behind all these instabilities is outlined in many papers (Dubois,1974; Forslund,Kindel and Lindmann,1975; Jorna,1974). Only the results will be quoted here. SRS and two plasmon decay are the most important for the work considered here.

The results for the one dimensional SRS can be gleaned from a number of papers. There is a summary of expressions for the threshold and growth rates for homogeneous or inhomogeneous

plasmas in Table I . V_o^2 is the quiver velocity defined by $e^2E_o^2/\omega_o^2/m^2$ and is found by $657\lambda^2(\mu)I(\ Wcm^{-2}\ )$. a_{ei} is the electron ion collision frequency $\approx 1.5\ 10^{-5}/T^{3/2}$. γ_L is the Landau damping constant $=-.22\ \sqrt{\pi}\omega_p{}^4\exp(1/(-2k^2\lambda_D{}^2))/(k^3V_E{}^3)$. ω_p is the plasma frequency and equals $\sqrt{(4\pi ne^2/m)}$. ω_k is the frequency of the EPW and equals $\sqrt{(\omega_p{}^2+3\kappa Tk^2/m)}$. L is the density scale length defined for density n as $(1/n\ dn/dx)^{-1}$. The formulas are quoted from Chen (1974). . Upon substitution of typical numbers one finds that the threshold intensity is near $10^{13}\ Wcm^{-2}$ and that the growth constant (for $\exp(\gamma t)$) is near $10^{12}\ s^{-1}$.

From the frequency and wave vector matching conditions one can derive much information about the phase velocities and the densities at which SRS can occur. The calculations (see appendix) yield the following salient facts. (1) SRS can only occur if densities less than .25 n are present .(2) The phase velocity drops off as the density is decreased for Raman backscatter. N_{cR} is density at which the plasma frequency equals the incident laser frequency. The laser light cannot penetrate into regions where the density is greater than n_{cR} . The phase velocity is found to be

$$V_{ph}/c = \sqrt{(1/((n_{cR}/n-1)\xi^{-2})+3\kappa T/(mc^2))}$$

and ξ is the solution to

$$\xi^2-2\xi+(2a\sqrt{(1+3\kappa T/(mc^2)\xi^2(a^2-1))}-1-3\kappa T/(mc^2)\xi^2(a^2-1))/(a^2-1)=0 \quad \text{where } a=\sqrt{(n_{cR}/n)}$$

. Since $\kappa T/(mc^2)$ is much less than 1 the cold plasma approximation can be used : T=0. If one defines a temperature by $\kappa T_{HOT}=mV_{ph}{}^2/2$ one can find κT_{HOT} as a function of density.

Table I Stimulated Raman Scattering :Formulas

Paper	Threshold Intensity	Growth Constant
Forslund Kindel Lindmann	$\frac{V_0^2}{c^2} > \frac{8(\omega_0-\omega_k)\gamma_L\, a_{ei}\, \omega_p^2 \omega_k^2 \omega_0}{2c^2k^2\omega_p^2\omega_0\,\omega_k(\omega_0-\omega_k)^2}$	$\gamma = \frac{kV_0\omega_p}{(\omega_k(\omega_0-\omega_k)8)^{1/2}}$
Lee Kaw	$\frac{V_0^{3/2}}{c^{3/2}} > \frac{.52^{3/2}}{k_0 L}$	$\gamma = \frac{V_0\omega_p}{2c}$
Jorna	$V_0^2 > \frac{16\gamma_R\,\omega_k^2\gamma_h}{k^2(\omega_0-\omega_p)\omega_p^2}$	$\gamma = \frac{V_0(\omega_0\omega_p)^{1/2}}{c}$
Chen	$\frac{V_0^2}{c^2} > \frac{2}{k_0 L}$	$\gamma = \frac{V_0(\omega_0\omega_p)^{1/2}}{c}$
Dubois	$> 10^9$ W cm^{-2}	$\gamma = \frac{E_0^2\omega_p\,\omega_k}{16\pi\, n\omega_0 \nu T(\omega_0-\omega_p)}$
Kruer	$> \frac{5\ 10^{17}}{L_\mu^{4/3}\lambda_\mu^{2/3}}$	---------

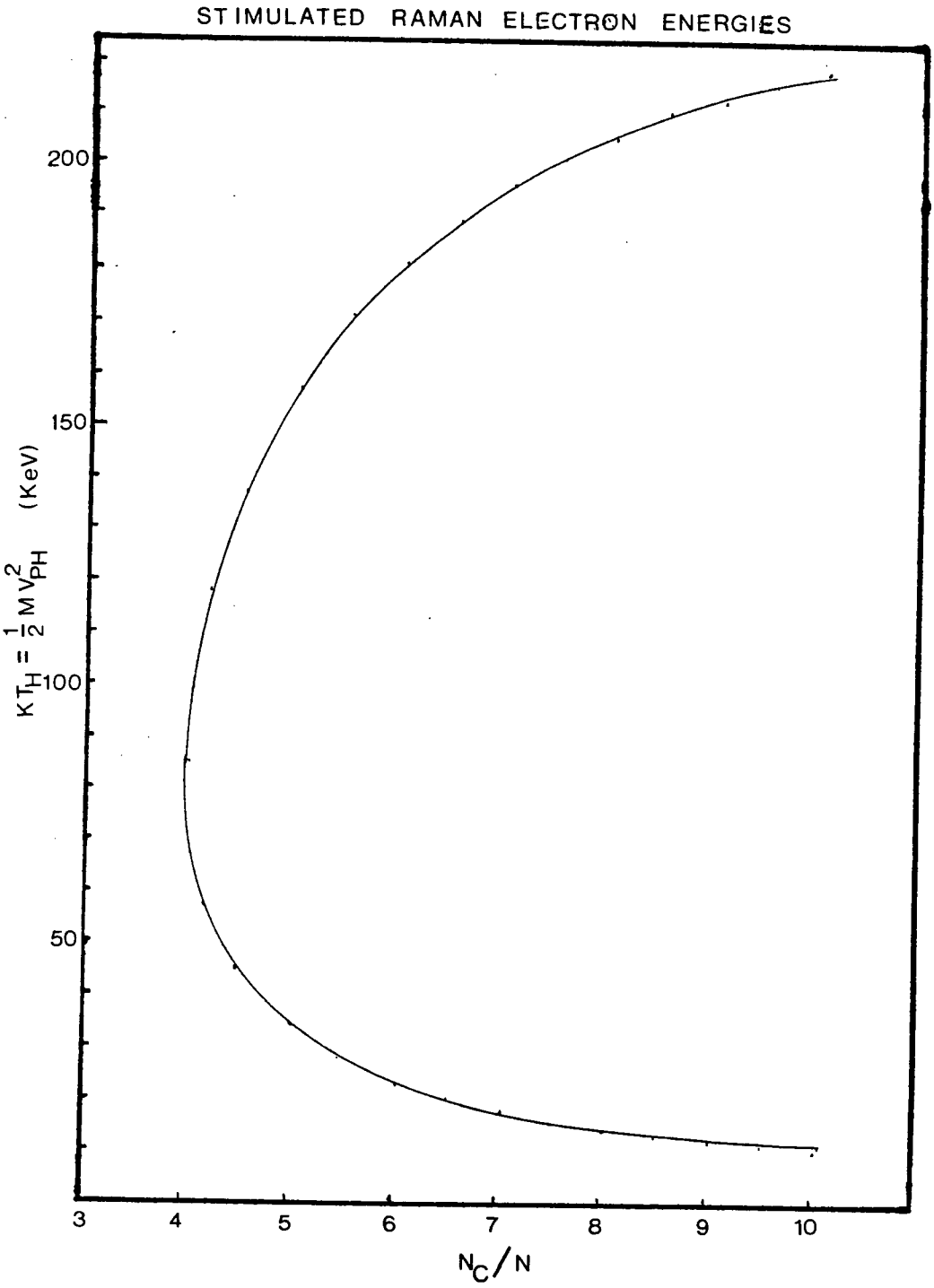
STIMULATED RAMAN ELECTRON ENERGIES
200
150
100
50
$KT_H = \frac{1}{2} M V_{PH}^2$ (KeV)
3
4
5
6
7
8
9
10
N_C/N

Figure II-1

This has been done and the results are plotted (Fig. II-1). Both forward Raman scattering (high energy) and backward Raman scattering (low energy) are plotted. Strictly speaking one should consider relativistic energies . The expression for κT in this case will be

$$\kappa T_{HOT} = mc^2((1+V_{ph}{}^2/c^2/\sqrt{(1-V_{ph}{}^2/c^2)})-1)$$

For V_{ph} at $.25n_{cR}$ one finds κT_{HOT} =115 keV. In both forward and back scattering the EPW generated propagates in the direction of the laser light wave vector ($+k_L$).

Once the phase velocity (or the k of the EPW) is known one can begin to estimate the number of electrons which may be initially trapped by the wave. One assumes that the background plasma can be described by a Maxwellian distribution at temperature κT. The electrons which are trapped have energies between $.5mV_{ph}{}^2-e\phi$ and $.5mV_{ph}{}^2+e\phi$. $E\phi$ was determined using Poisson's equation and is equal to $4\pi e\delta n/k^2$. These energies correspond to a range of velocities and thus upon a slight change of variables

$$x^2=.5mv^2/\kappa T$$

we find that

$$n_{TRAP} = n_o(\mathrm{erf}(x_u)-\mathrm{erf}(x_L))$$

$$x_u=\omega/k\sqrt{(m/(\kappa T))}+\omega_p/k\sqrt{((\delta n/n_o)m/(\kappa T))}$$

$$x_L=\omega/k\sqrt{(m/(\kappa T))}-\omega_p/k\sqrt{((\delta n/n_o)m/(\kappa T))}$$

The absolute number of electrons generated has also been estimated by computer simulation (Hiob and Barnard, 1983). For $(V_o/c)^2=.0625$, 3 % of the electrons in the plasma are converted

Exponential growth cannot continue indefinitely . Since it is the amplitude of the electrostatic wave which is growing one should examine the mechanisms which prevents further growth. Trapping of electrons in large amplitude waves (Ichimaru,1973) has been proposed as a mechanism which prevents further growth. In this case further energy input goes into electron kinetic energy (fast electrons) and not into the growth of the wave amplitude.

Modification of the scale lengths and coupling into ion acoustic waves in the plasma has also been proposed as a saturation mechanism . If the waves grow too large , pondermotive forces of the decay EPWs couple and cause the scale length to shorten (Langdon and Lasinski,1976; Estabrook and Kruer,1983). This means unless the laser intensity can increase fast enough to compensate for this decrease in scale length the threshold condition will soon be exceeded and the growth stops. The wave will then damp away.

The shape of the distribution function is also important. From the simple theory of trapping one might expect a distribution centered on the phase velocity and decreasing locally away from this center. This would assume that there are no randomizing collisions. From a discussion of the relaxation times (Spitzer,1962) one can estimate the time needed to thermalize a distribution of electrons. For T=1 keV and n= $.25n_{CR}$ one finds the time necessary is about 5 ns. This means the background plasma has time to thermalize. For T=80 keV the

time necessary is greater than 400 ns. This is much longer than the laser pulse and hence we would not expect a Maxwellian distribution. It is interesting to note ,however, that computer simulations predict that a Maxwellian distribution results (Estabrook, Kruer and Lasinski,1980) at a hot temperature equal to the phase velocity energy. The mechanism behind this is not understood.

The time evolution of the electron signal has been followed in computer simulations (Hiob and Barnard ,1983). The results indicate that the fast electrons appear rapidly (ω t about 50) after the threshold intensity has been reached in the pulse and remain constant thereafter.

The other parametric instability of importance is the two plasmon decay. The theory of this decay has been covered by a number of researchers (Jackson,1967; Liu and Rosenbluth,1972; Langdon and Lasinski,1978;Simon,Short,Williams and Dewardre). The results of these and others are condensed in table II. Substitution of numbers yields thresholds near 10^{12} W cm^{-2} and growth rates near 10^{12} s^{-1} .

The electron plasma waves generated have a maximum growth rate near 45 degrees with respect to the laser beam axis in the plane of polarization .

The ks of the two plasmon EPWs are usually initially much greater than k_o. This would suggest that the mean energy of the generated fast electrons (κT) would be much less than $.5m(\omega/k_o)^2$=85 keV. For $k=2k_o$ this would imply a κT about 20 keV

Table II Two Plasmon Decay :Formulas

Paper	Threshold Intensity	Growth Constant
Liu Rosenbluth	$\frac{V_0^2}{V_e^2} > \frac{3}{k_0 L}$	$\gamma = \frac{k_0 V_0}{2} - \frac{\omega_p}{k_y 2L}$
Jackson	$E_0 > \frac{16\omega_p^2 m\gamma_l}{k_0\ \omega_p}$	$\gamma = \frac{e\vec{k}\cdot\vec{E}_0\vec{k}\ \cdot\vec{k}_0}{8mk^2\omega_p}$
Rosenbluth	$I(W\ cm^{-2}) > \frac{T(KeV)}{600L(mm)}$	$\gamma = \frac{(e^2\pi I)^{\frac{1}{2}}}{(2m^2c\beta)^{\frac{1}{2}}}$
Simon et al.	$\frac{V_0^2}{V_e^2} > \frac{3}{k_0 L}$	---------
Kruer	$I(W\ cm^{-2}) > \frac{T(eV)\,10^{13}}{L\lambda_\mu}$	---------
Dubois	$> 10^9$ W cm^{-2}	$\gamma = \frac{E_0^2\vec{k}\ \cdot\vec{k}_0\vec{k}\cdot\vec{E}_0\,\omega_p}{32\pi n\kappa Tk^2 k_y E_0}$

assuming that .5 $mV_{pH}^2 = \kappa T$. However soon after surpassing threshold there appears a rapid decay into shorter k waves (Baldis and Walsh,1983). This implies that a higher κT actually observed experimentally is not unreasonable.

The frequency of these waves is about $\omega_p = \omega_o/2$. The waves can scatter the incident laser at a frequency = $\omega_o/2 + \omega_o = 3/2\ \omega_o$. This scattered radiation can be detected and is usually considered a sign that two plasmon decay is occurring.

Other Mechanisms

Other mechanisms have been proposed to generate fast electrons. These however usually predict much lower temperatures than observed herein. For completeness, these methods will be briefly mentioned.

Filamentation can generate fast electrons in underdense plasmas. The incident laser can be further focused by the plasma it creates. It is this much higher local intensity which generates the fast electrons via parametric instabilities (Cohen and Max ,1979; Ng et al,1979; Herbst et al,1981).

Both ion acoustic and electron plasma wave turbulence have been proposed . Turbulence in this context describes the randomization of wave vectors from an initially nearly ordered state. EPW turbulence has been predicted to generate a Maxwellian distribution at 20-30 keV (Silin and Tikhonchuk ,1981). Ion acoustic turbulence has been shown in computer simulations to generate a distribution characterised by a

$T_{HOT} = 1.5/(1-n/n_{CR}) * T_{COLD}$ (Estabrook,1981). For our conditions this would imply $T_{HOT} = 4$ keV.

Resonance absorption is the process in which laser light penetrates to the critical density layer of the plasma at an oblique angle with an electric field component parallel to the density gradient and drives a purely exponentially decaying wave into the plasma. There are numerous papers which describe resonance absorption (Estabrook and Kruer,1978; Forslund,Kindel and Lee,1977; Kolodner and Yablonovitch,1976). These papers theoretically predict or report measurements of 10-20 keV Maxwellian distributions for the fast electrons. This is not an important process in our case since we do not reach critical density in our plasma.

CHAPTER 3 EXPERIMENTAL SETUP

The investigation of SRS in the laser plasma interaction described in this report uses 3 basic components : a CO_2 laser, the gas jet target and the diagnostics. These will now be discussed in detail.

To study parametric processes in laser plasma interaction one must first find an appropriate laser. From the theory previously discussed one basic parameter is the quiver velocity of an electron in the laser's electric field given by $V_o^2=e^2E_o^2/(\omega_o^2m^2)$ or proportional to $I\lambda^2$. We also know that this term must be relatively large (about 10^{15} μm^2 Wcm^{-2}). A CO_2 laser is ideal since its long wavelength at 10.6 μm means that the required intensity is about 10^{13} W cm^{-2} which is much more easily reached than the 10^{15} Wcm^{-2} required if one was to use 1 μm light. The CO_2 laser used at UBC is capable of producing the intensities required to study SRS and other parametric processes.

The CO_2 Laser System

The CO_2 laser system is outlined on Fig III-1. It was set up by J.Bernard, J.Cherwoniak, C.J.Walsh, H.Houtman, R.Popil and J.Meyer . Distances between mirrors (in cm) are indicated . The system can be described as follows. The longitudinal mode and the tranverse mode are fixed by the CW HP (collectively known the hybrid laser) section. The HP stands for high pressure and CW stands for continuous wave laser. This combination is used to create a single mode 100 ns gain switched

pulse generated when an electrical discharge in HP creates a population inversion in that section and thus changes the gain. The polarization is fixed by Brewster windows within the cavity and by the germanium polarizers GP located outside the cavity. The wavelength is fixed by a temperature controlled germanium etalon used as the output coupler at the exit of the CW section. The Pockel's cell is arranged so that with no voltage applied to it the pulse will pass through the germanium flat G and be reflected into the Optical Engineering Spectrum Analyzer SA. A 2 ns pulse of high voltage is applied to the PC . This causes the plane of polarization to rotate by 90 degrees . Since G is set at the Brewster angle this new polarization will be reflected off G and into the rest of the system. This 2 ns HV pulse is applied near the peak of the gain switched pulse. This pulse also provides a convenient timing pulse to be used to trigger diagnostics later in the system.

The 2 ns pulse passes through lens L1 which focuses the beam onto a polyethylene sheet PS. There is no breakdown at the sheet and the pulse continues on through lens L2. The lens combination L1-L2 has a focus at F1 where a spatial filter is located. F1 has two purposes : first to clean up the beam going into the K103 preamplifier and second to provide a breakdown point for the backscattered beam from the laser target .

The pulse is amplified by the K103 preamplifier. It passes through L3 which focuses the pulse into a second spatial filter F2. F2 also has provision for spark breakdown timed so that the incident pulse can pass through unimpeded. The backscattered

UBC CO_2 LASER

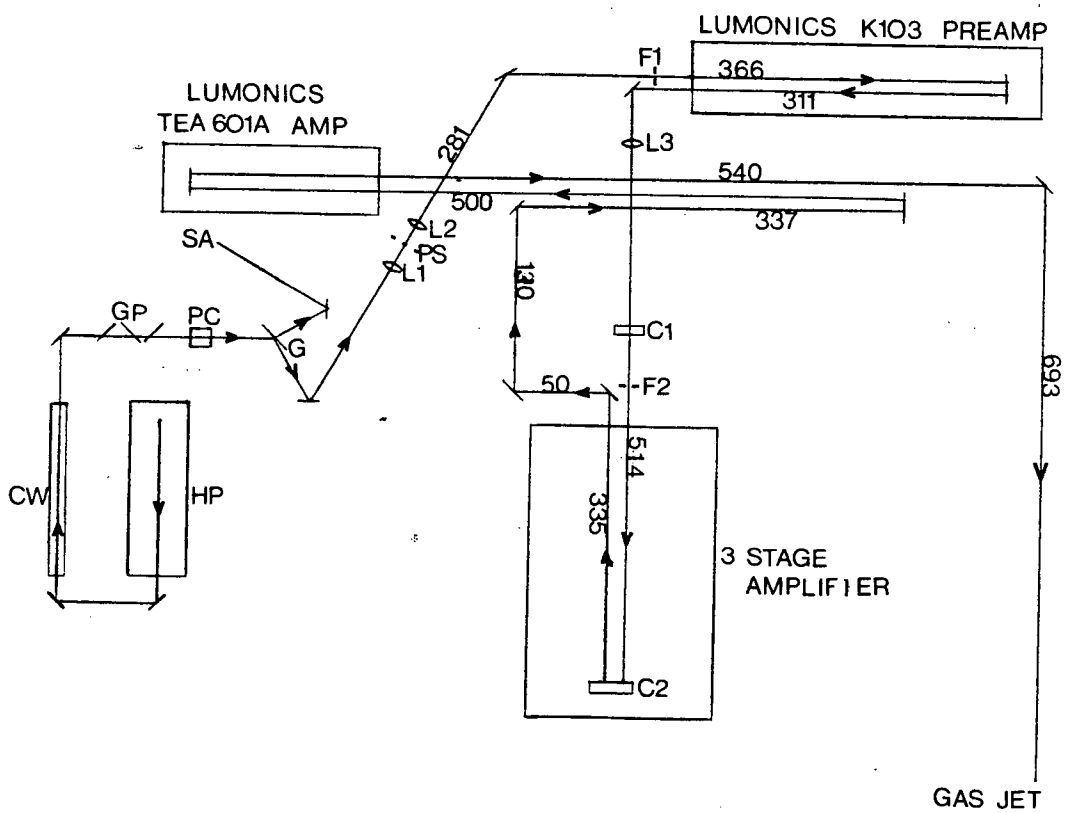

Figure III-1

pulse will find a dense plasma when it attempts to pass through this point and hence will be attenuated by refraction and absorption. The pulse is amplified by the three stage amplifier. This is a lab-built 3 module amplifier described in UBC Plasma Physics Report No.79 (Houtman and Walsh). The beam is amplified again by a commercial Lumonics amplifier module and the amplified beam is sent to the gas jet target.

The imperfect contrast ratio of the Pockel's cell has been compensated for in the system. A problem arises because not all of the 100 ns pulse is perfectly rejected when the 2 ns pulse is switched out. This provides wings on the laser pulse which are of low intensity, but contain a substantial amount of energy. The problem is known to be eliminated when no energy is detected after the laser is fired with no 2 ns pulse applied to the PC. This is accomplished by filling gas cell C1 with 4-15 Torr of SF_6 and 760 Torr of He in an approximate distance of 2 cm. He. It is also important to prevent self-lasing in the laser by making the rear mirror of the three stage invisible to low intensity CO_2 radiation. This is done by filling the gas cell C2 with 1-1.5 Torr SF_6, 20 Torr ethanol, 100 Torr Freon and 640 Torr of He. Both cells work on the principle that SF_6 is a saturable absorber. This means that low intensity radiation is absorbed, but high intensities cause the SF_6 to bleach and permit the passing of the radiation. The properties of SF_6 have been measured by other researchers (Burak et al,1969).

Cross sectional quality of the beam to be focused onto the gas jet is not perfect. Although the beam is assumed to be

Gaussian , for the calculation of the focal spot radius , evidence from the thermal paper indicates that there are a few irregularities in the beam. These results must be interpreted carefully since the response of the thermal paper is decidely non-linear. The structure is due to the non-uniformity of the discharge in the amplifiers. The structure however is not important for these long wavelengths. The measurement of the focal spot size using a two dimensional grating technique(see Bernard Ph.D. Thesis 1984) indicates the typical focal spot size is 46 μm waist radius .

The laser is thus able to provide a pulse of CO_2 radiation at wavelength 10.6 μm with energies in the range 0-15 Joules and in a time typically 2 ns fwhm. With the f/5 focusing lens intensities approaching 10^{14} W cm^{-2} may be reached.

The parameters describing the CO_2 pulse were determined as follows. The wavelength was noted for every shot on the spectrum analyzer; the incident energy was measured using a photon drag IR detector (calibrated every experimental session); the transmitted energy was noted using an Apollo energy meter ; and the pulse length and shape were noted by displaying the photon drag signal on a Tektronix 7104 oscilloscope.

With the laser pulse we now can proceed to study laser plasma interactions. The plasma can be formed by a laser pulse striking a target or it can be preformed as in a z pinch.

The Gas Jet Target

The gas jet target is based on a design from the National Research Council in Ottawa and the University of Alberta . It was set up at UBC by R.Popil and A.Ng. It uses a Laval nozzle to produce a laminar jet of nitrogen gas. The Mach line calculations based upon Giles (Ph.D,1983) and Shapiro (1953) indicate that we should have a laminar jet of uniform molecular density (within 10 %) (see Fig III-2) . A Mach line is a boundary between different flow regions in the gas jet. The calculations of the Mach lines themselves depend only on the initial Mach number (at the exit) and the pressure ratio between the background and the reservoir. The throat width A* and the exit width A of the gas jet nozzle are indicated in the diagram. For these dimensions a Mach number M of 4.51 can be reached at the exit. This assumes that there is isentropic flow. This Mach number can be calculated from the formula

$$(A^2/A^{*2})=(2/(\gamma-1)(1+M^2(\gamma-1)/2))^{((\gamma+1)/(\gamma-1))}/M^2$$

(from Chorlton,1967). γ is the ratio of the specific heats and is usually taken as 1.4 . The density n at the exit (region 1) can also be calculated using another formula from Chorlton .

$$n_o/n=(1+M^2(\gamma-1)/2)^{1/(\gamma-1)} \quad (no=reservoir\ density)$$

Substituting numbers one finds $n/n_{CR}=(2Z_{AVE})2.67/57.82$ for STP conditions in the reservoir. Assuming the nitrogen is fully ionized the 5 Torr jet should have $n=1.43\ n_{CR}$. This is after converting from STP conditions to ambient conditions in the reservoir. In region 2 the Mach number can be calculated if one realizes that the pressure in this region is the same as the ambient pressure P_B of the background He. Assuming the pressure in region 1 is the same as in the reservoir P_R, the isentropic

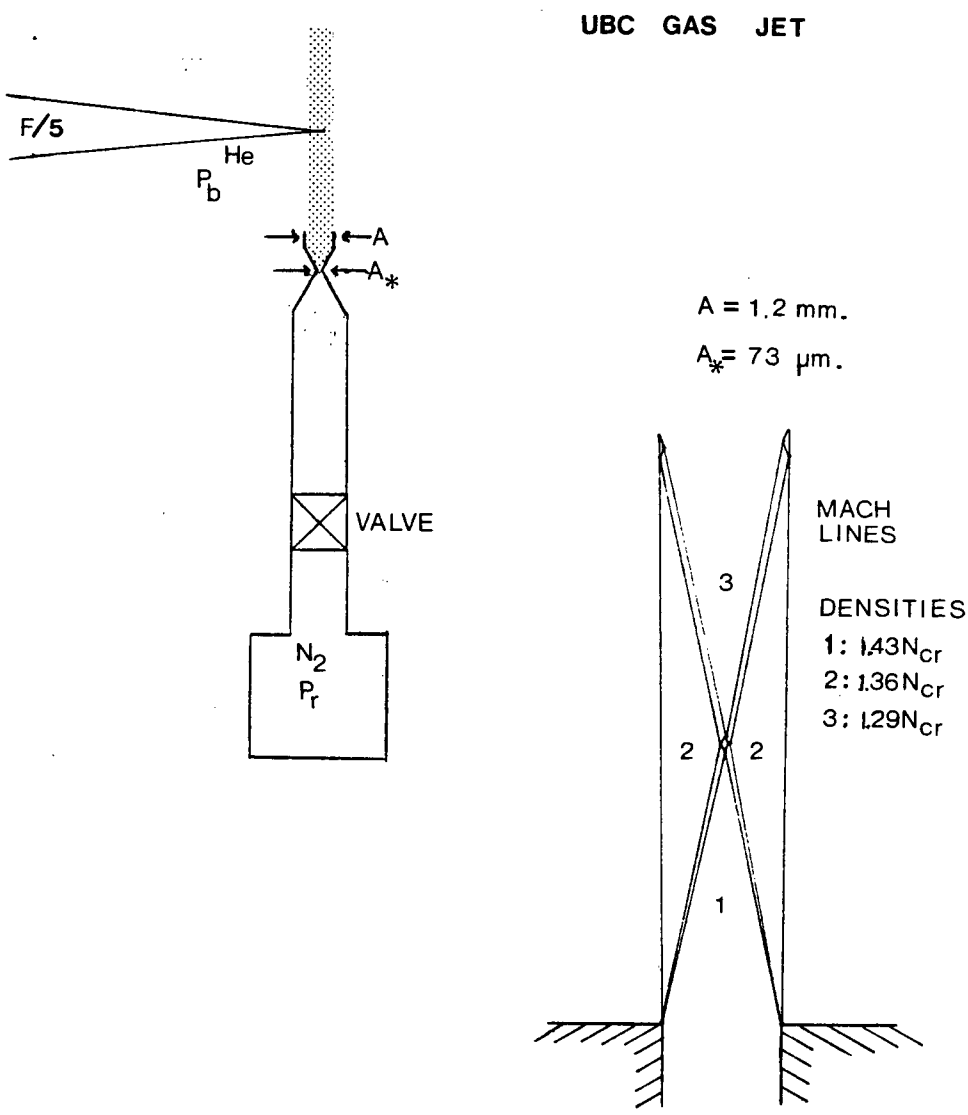
UBC GAS JET
F/5
He
P_b
A
A_*
A = 1.2 mm.
A_* = 73 μm.
VALVE
N_2
P_r
MACH LINES
DENSITIES
1: 1.43N_{cr}
2: 1.36N_{cr}
3: 1.29N_{cr}
1
2
2
3

Figure III-2

pressure relation

$$P_R/P_B = (1+.5M^2(\gamma-1))^{**}(\gamma/(\gamma-1))$$

will yield the the Mach number. Substituting the pressure ratio used in the experiment ($P_R/P_B = 314$) we find that M=4.56 ie the same Mach number as in region 1. By the n_o/n formula above this implies that there is almost the same density in regions 1 and 2. For densities further up in the jet (region 3 and beyond) the method outlined in Shapiro can be followed. The density in region 3 should be 1.29 n_{CR} . The densities calculated are above the measured densities since hydrodynamic motion and incomplete ionization can occur. These will tend to lower the density.

The relationships indicate that the molecular density in the jet is linearly related to the density in the reservoir and assuming the ideal gas law to the pressure in the reservoir. Thus we have a convenient way of controlling the maximum density the laser can see. Since also the background pressure is linearly related to the reservoir pressure for stable gas jet conditions one can label the density region to be explored by specifying the background pressure. In our case , this is valid as long the nozzle remains the same. Since .4 n_{CR} is reached with a 5 Torr background 3/5 x .4 n_{CR} will be reached by a 3 Torr background jet ie .25 n_{CR} . This assumes that the average Z remains the same and that the same hydrodynamic motion occurs for both jets.

One thing in the diagram of the gas jet not indicated explicitly is the throat which connects the reservoir to the nozzle. This is the actual 'reservoir' filled by opening the

reservoir valve. The pressure to which this is filled depends upon the amount of gas released from the reservoir. This in turn depends on how long the reservoir valve has been opened. Since a manual valve push button is used there is some variation in the time the valve is open. This time is reproducible for an individual but not from individual to individual. The effect manifests itself directly in the final reservoir pressure :the longer the valve is open the lower the reservoir pressure. The implication is that the jet conditions are affected by the length of time the valve is open. This has been observed for xray emission under different conditions.

The basic plasma parameters are as follows: temperatures around 2 keV and 300 eV (Popil Ph.D. Thesis 1984) determined by xray absorption foil techniques (Popil and Meyer,1981), densities near .25 n_{CR} reaching .4 n_{CR} maximum and typical scale lengths of 300 μm. The last two parameters were determined by interferometry using a Jamin interferometer.

The Spectrometers

The third element required to study SRS is diagnostic equipment. In this case two electron spectrometers were built, MK II a single channel (variable energy) and MK III a four channel system.

MK II is the single channel spectrometer built to study the fast electrons produced by the laser interaction with the gas jet at UBC. It is a basically simple device. It consists of an electromagnet (Helmholtz configuration) ,an entrance aperture

and a detector situated at 90 degrees. The size and other details of the construction are shown in Fig III-3 the theory of its operation is quite simple (at least to first order). One assumes a uniform magnetic field within the radius of the coils and zero magnetic field exterior to the coils. This is a good approximation (Livingood) provided one uses an effective radius. For the Helmholtz coil the effective radius is near the physical radius. The calculated field in the median plane and the measured field in the same plane are shown in Fig III-5a. The calculated field was found by merely integrating the the expression

$$B= \mu_o I/(4\pi) \int \nabla \times \vec{r}/r^3 \, dr \quad .$$

With the magnetic field given by the expression

$$B= 8\mu_o NI/(\sqrt{125}\ r) \text{ (at center of midplane)}$$

and the following

$$evB=vp/r$$

we can solve for p=eBr and find the relativistic kinetic energy

$$E=mc^2(\sqrt{(1+(eBr/(mc))^2)}-1)$$

where I= current in magnet e=charge on electron m= mass of the electron r=radius of the orbit (same as physical radius if entrance and exit are at 90 degrees). The expression for B as a function of I was checked and found to be as predicted (within 10 %)

The focusing properties of the magnet are hard to judge experimentally. However Livingood does give good expressions for the theoretical properties. Trajectories for electrons of the same energy entering the aperture are indicated in the diagram. The energy resolution is approximately +/- dR/R. This

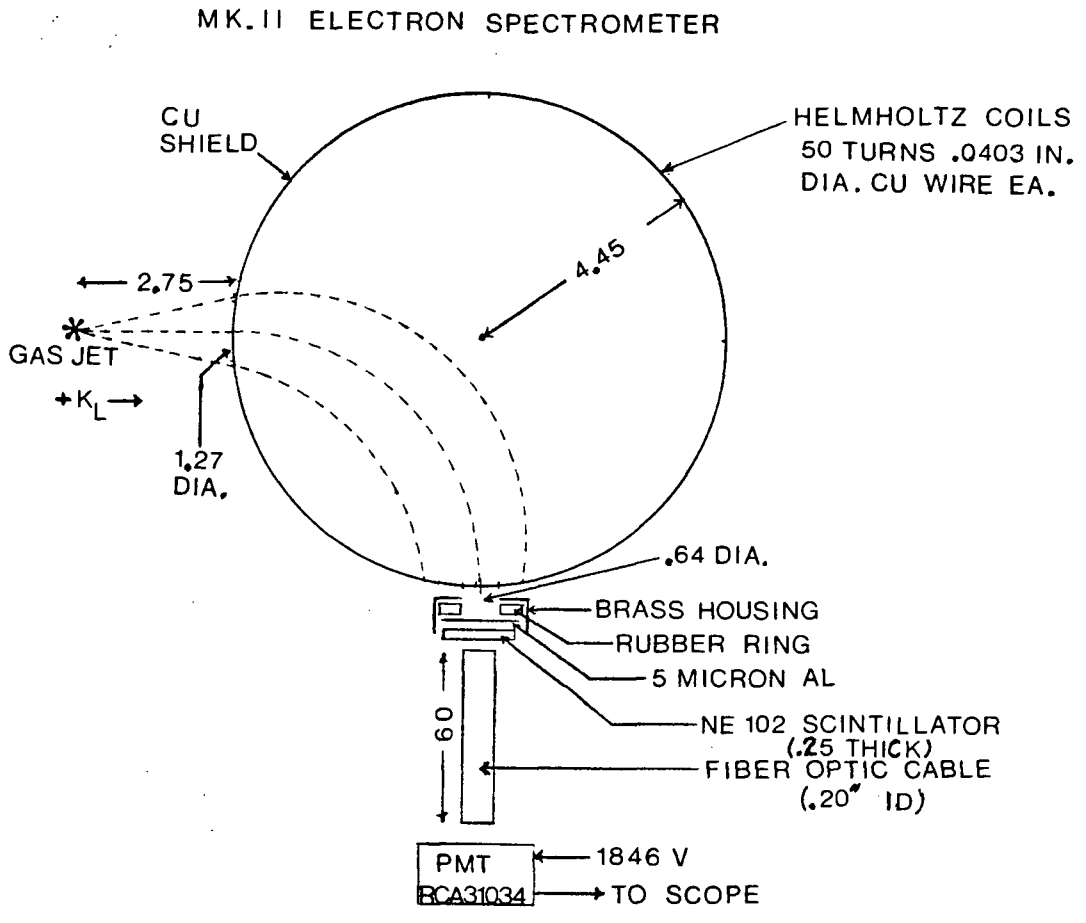

DIMENSIONS IN CM
UNLESS INDICATED
OTHERWISE

Figure III-3

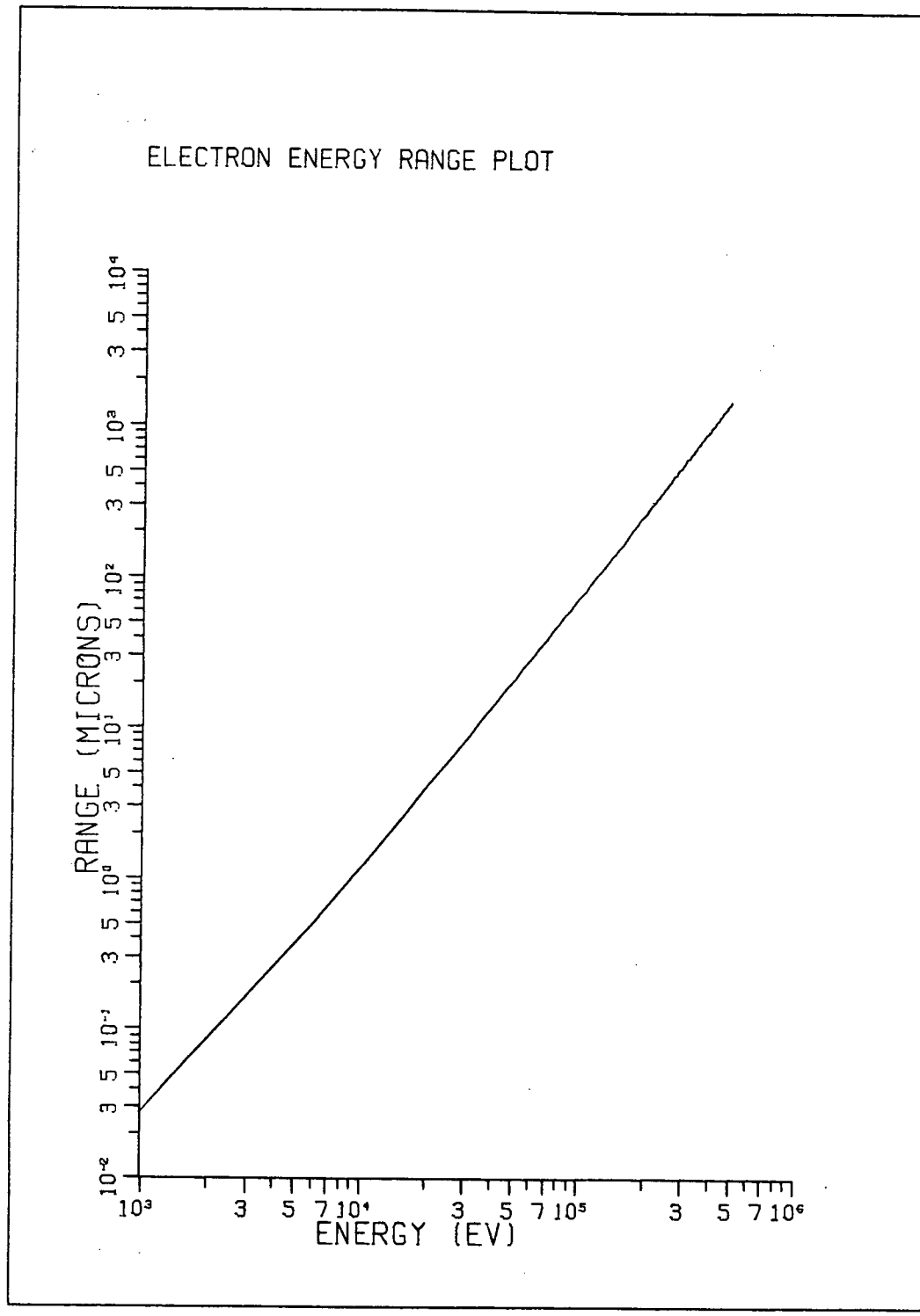

Figure III-4

corresponds to +/- 15%. The solid angle subtended is fixed by the exit aperture area A and the distance D from the gas jet to the exit aperture. The solid angle is A/D^2. With A=.32 cm^2 and D=9.74 cm the solid angle is 3.37 10^{-3} sr.

The detector used was a simple foil-scintillator-optical fiber-photo multiplier combination . A 5 μm aluminum foil (obtained from Goodfellow Metals, Cambridge,England) was placed in front of NE 102 plastic scintillator and the scintillator light was guided by a 60 cm optical fiber to an RCA 31034 photomultiplier. The signal was sent to a Faraday cage screened room and displayed on an oscilloscope.

More elaborate spectrometers based upon a Thomson parabola were considered, but had to be rejected since, for the energies and dimensions required, the electric field needed was large enough to cause glow discharges in the 5 Torr background helium.

The 5 μm foil does present a problem as not all the electrons will penetrate it. Calculations based on the integration of the energy loss formula (Segre,1977)

$dE/dx=2\pi e^4 n \ln(E/Ion)/E$ (Ion=9.1Z/(1+1.9Z**-.667)(eV))

indicate that for 50 keV electrons most of the electrons make it through the foil with less than 10 % energy loss (see Fig III-4). The foil has two effects on the electrons. It attenuates the the number of electrons passing through it by an amount exp(t/r(E)) . It also reduces the mean energy of the electrons passing through the foil. A further complication is that xrays are generated as an electron loses energy in the foil; these can subsequently be detected by the scintillator. Any losses due to

xray emission are neglected in the analysis.

The response of the NE102 scintillator has been measured for low energy (less than 10 keV) electrons and was found to be linear (von Schmeling,1960). The response to low energy xrays has also been measured and was also linear with energy (Meyerott,1964). This has also been confirmed by measurements for this work. It is assumed that the response is linear to higher energies. This assumption is true provided dE/dx is small. The correct expression is

$dS/dx=adE/dx/(1+kb\ dE/dx)$ where kb = .01 g cm^{-2} Mev-1 and is approximately adE/dx if kb dE/dx much less than 1. S is the signal due to fluorescence (Prescott et al,1961)

The optical fiber is a good quality fiber obtained from Welch Allyn ,Skaneateles Falls N.Y . The attenuation coefficient measured for the scintillation light (wavelength of maximum output 423 nm) is .032 cm^{-1}. This results in an 85% signal loss in the fiber.

Some efforts were made to eliminate noise from the PMT signal. These included using double shielded coaxial cable for the signal and HV lines. The PMT was encased in a copper metal box and isolated from the box by Mylar plastic. The box was mounted on a Plexiglass stand, isolated from the jet housing. The HV supply however was kept outside the screened room. In spite of these efforts the noise level was about 100 mV or less. This means that small signals could not be unambiguously sorted out and are therefore not analyzed.

MAGNETIC FIELDS

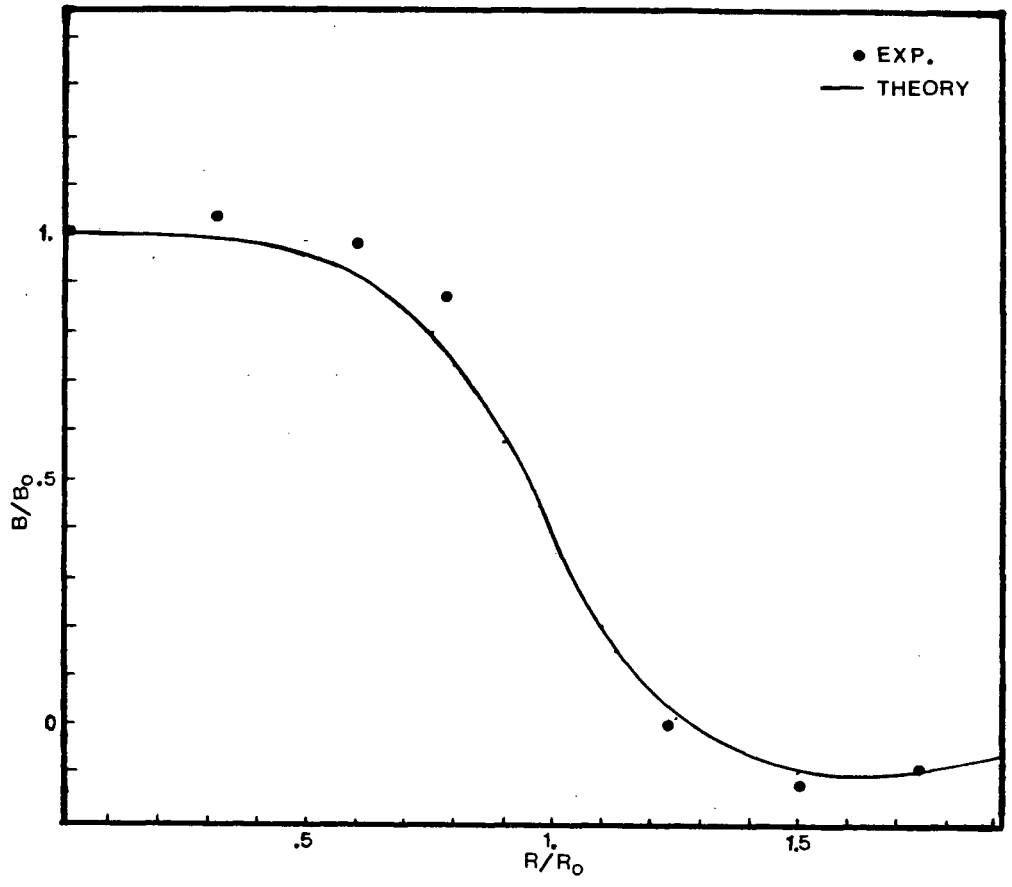

a. MK II

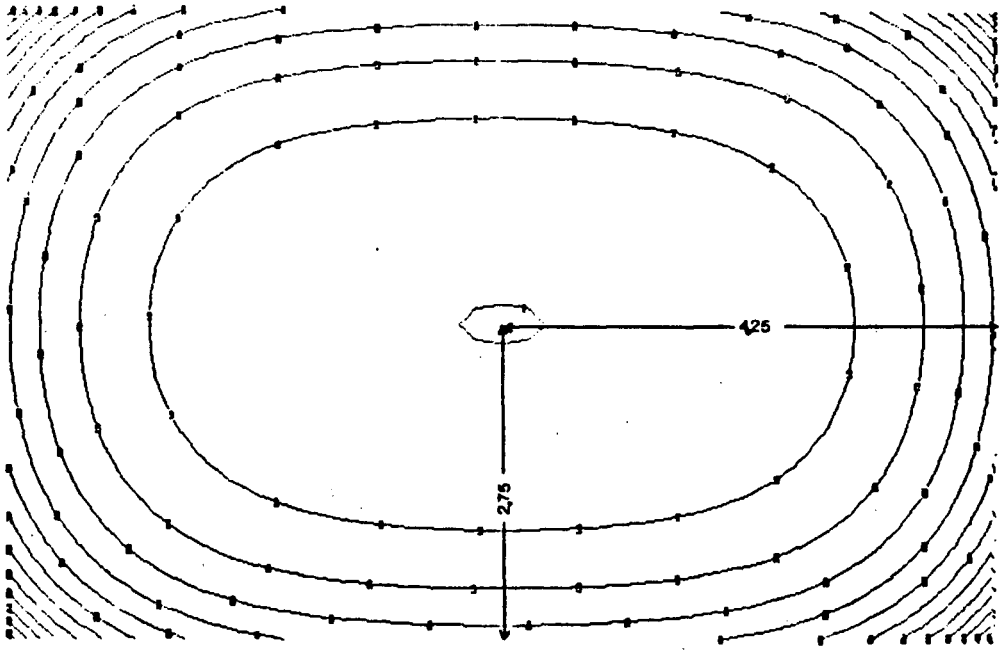

b. MK III Figure III-5

MK III is the 4 channel spectrometer. It is an iron core electromagnet based spectrometer designed to produce a large field and examine high energy electrons (up to 300 keV). The four channel aspect is important since there are large shot to shot variations in the electron signal. This makes the analysis of the single shot single channel data very difficult and one cannot derive with an effective electron distribution. The side view is shown in Fig III-6 . Trajectories of electrons in an assumed uniform magnetic field are shown. The location of the scintillators was chosen so that the best focus was obtained. The calculated magnetic field at the midplane for only the coils is given in Fig III-5b. The center contour line is a 110 Gauss line and the contour interval is 30 Gauss. The field was calculated for a 10 Ampere current in the coils. The actual field is smoother and slightly (x1.2) stronger than predicted. The iron exterior construction was originally intended to provide a more uniform field. As in the single channel spectrometer the detector consists of a foil- scintillator combination. The foil is 5 μm thick and the scintillator is NE102 plastic scintillator. The channels are connected via optical fibers to the head of an Optical Multichannel Analyzer(OMA) Model 1205I manufactured by Princeton Applied Research Corporation. The relative response was measured by using attenuated room light.

The OMA requires some timing considerations as it reads the channels sequentially. To synchronize the laser light pulse, the gas jet and the OMA read cycle properly a two channel delay unit was used. The timing pulse from the OMA triggered both the

MK. III ELECTRON SPECTROMETER

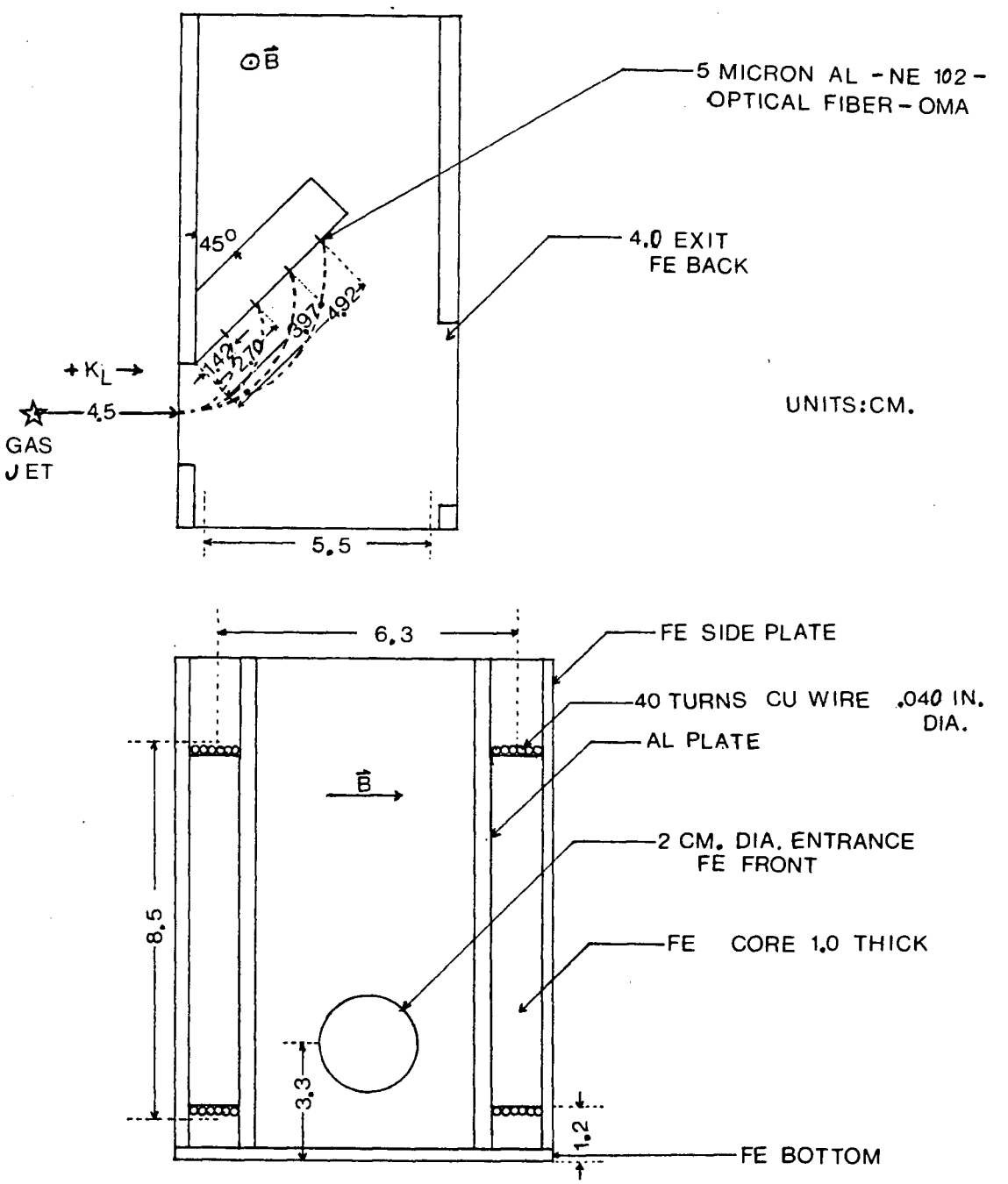

Figure III-6

jet and the laser independently (after both signals have gone through the delay units). The jitter of the jet with respect to the laser is less than 1 ms which is acceptable since the jet is stable for several tens of ms. The trigger to the jet is also accurately reproducible (length 150 ms.) hence eliminating the potential problem of the manual pushbotton firing of variable time length.

CHAPTER 4 EXPERIMENTAL RESULTS

The experimental results can now be presented. They will be presented in the following order: the signal level as a function of pressure , the signal as a function of laser intensity and the signal as a function of electron energy sampled. All errors bars are for standard deviations of the mean unless otherwise noted.

Pressure Dependence

The discussion of the variation of the number of electrons as the reservoir pressure is changed will be presented first. As can be seen from the graphs (Fig IV-1,2) the number of electrons grows very rapidly as the background pressure increases above 3 Torr. This is true both for electrons in the backward and forward directions. Since it is known that the maximum molecular density is proportional to the reservoir pressure the pressure axis could be relabelled as the average density axis. In this context the results take on a clearer meaning. The number of electrons seen in a given energy range increases dramatically as the amount of plasma near .25 ncr is increased.

Intensity Dependence

The background pressure can now be fixed and electron production as a function of laser intensity can be observed. The results are plotted for the 4 Torr and the 5 Torr jets (Fig IV-3,4). The scales are relative ; 10 units for the 4 Torr

results corresponds to 1 unit for the 5 Torr results. The error bars in the energy indicate the size of the bins used when averaging the data.

The plots are similiar. The signal starts off small at .5 10^{13} Wcm^{-2} , increases to a maximum signal near 4 10^{13} Wcm^{-2} and decreases to almost zero beyond 7 10^{13} Wcm^{-2}. The decrease is unexpected as one would naively expect the number of electrons to saturate, but not decrease.

If one assumes that a Boltzmann distribution is valid , an attempt at finding the so called hot electron temperature can be made by comparing signals at different electron energies. A couple of caveats must be made . There is no a priori reason that a Maxwellian distribution should be expected . Since the temperature calculated depends critically on the relative sizes of the two electron energy signals , small errors will have dramatic results on the temperature calculated.

By normalizing the signals (ie dividing by the energy examined $n=S/\xi$) one gets the relative number of electrons at a particular energy. Since for a Boltzmann distribution $n(\xi)= no\sqrt{\xi}exp(-\xi/\kappa T)$ two normalized signals can be used to find $\kappa T=(\xi 1-\xi 2)/ln(n1\sqrt{\xi 2}/(n2\sqrt{\xi 1}))$. The experimental results indicate that $n1/n2 = 1.27+-.67$ for the 5 Torr jet at 4 10^{13} W cm^{-2}. This means that,since $\xi 1-\xi 2$ = 50 keV, κT will be 85+-220 keV. The large error is due to the logarithm in the calculation of κT.

One qualitative observation to be made is that ,for the 4

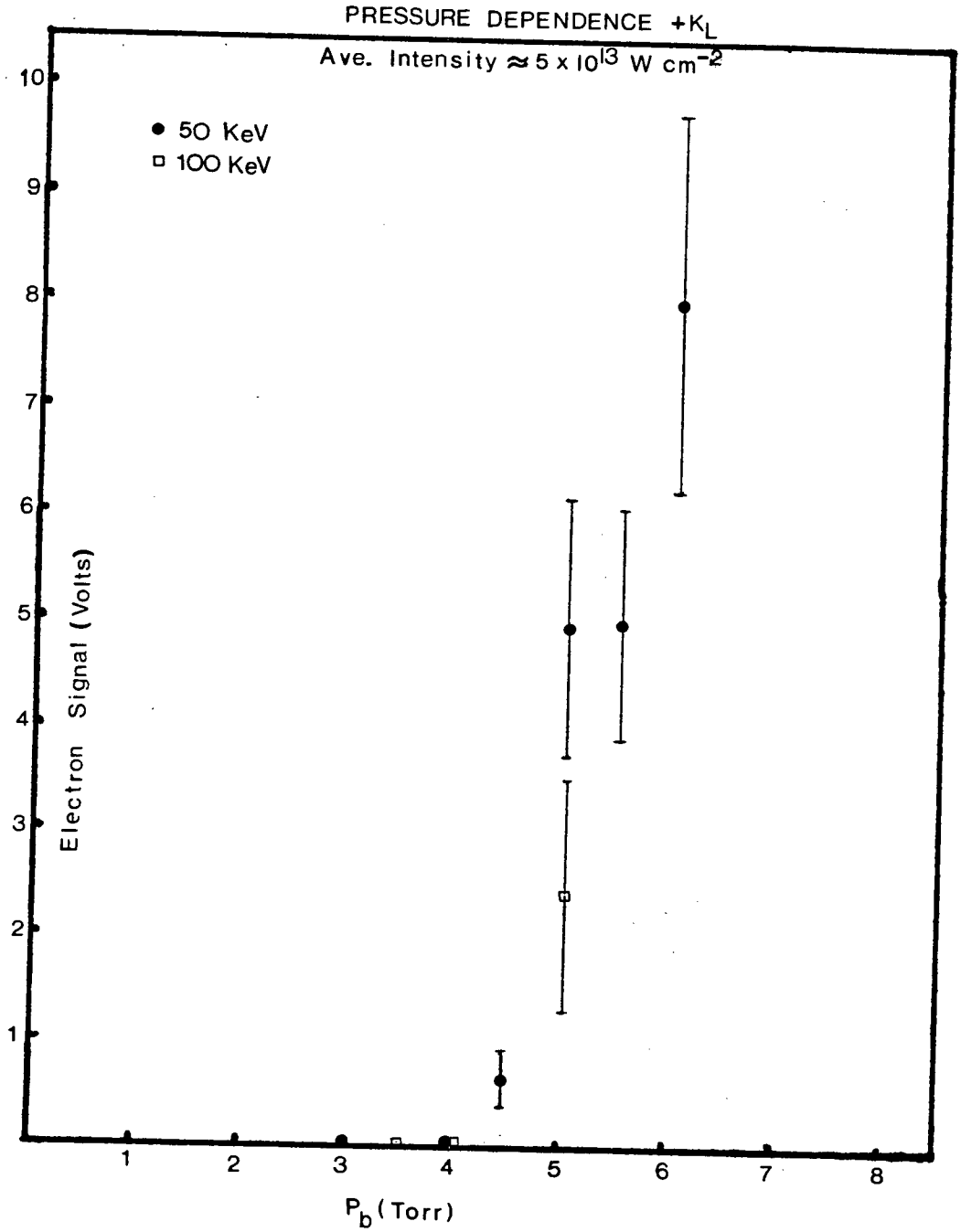
PRESSURE DEPENDENCE +K_L
Ave. Intensity ≈ 5 x 10^13 W cm^-2
● 50 KeV
□ 100 KeV
Electron Signal (Volts)
P_b (Torr)
1
2
3
4
5
6
7
8
9
10

Figure IV-1

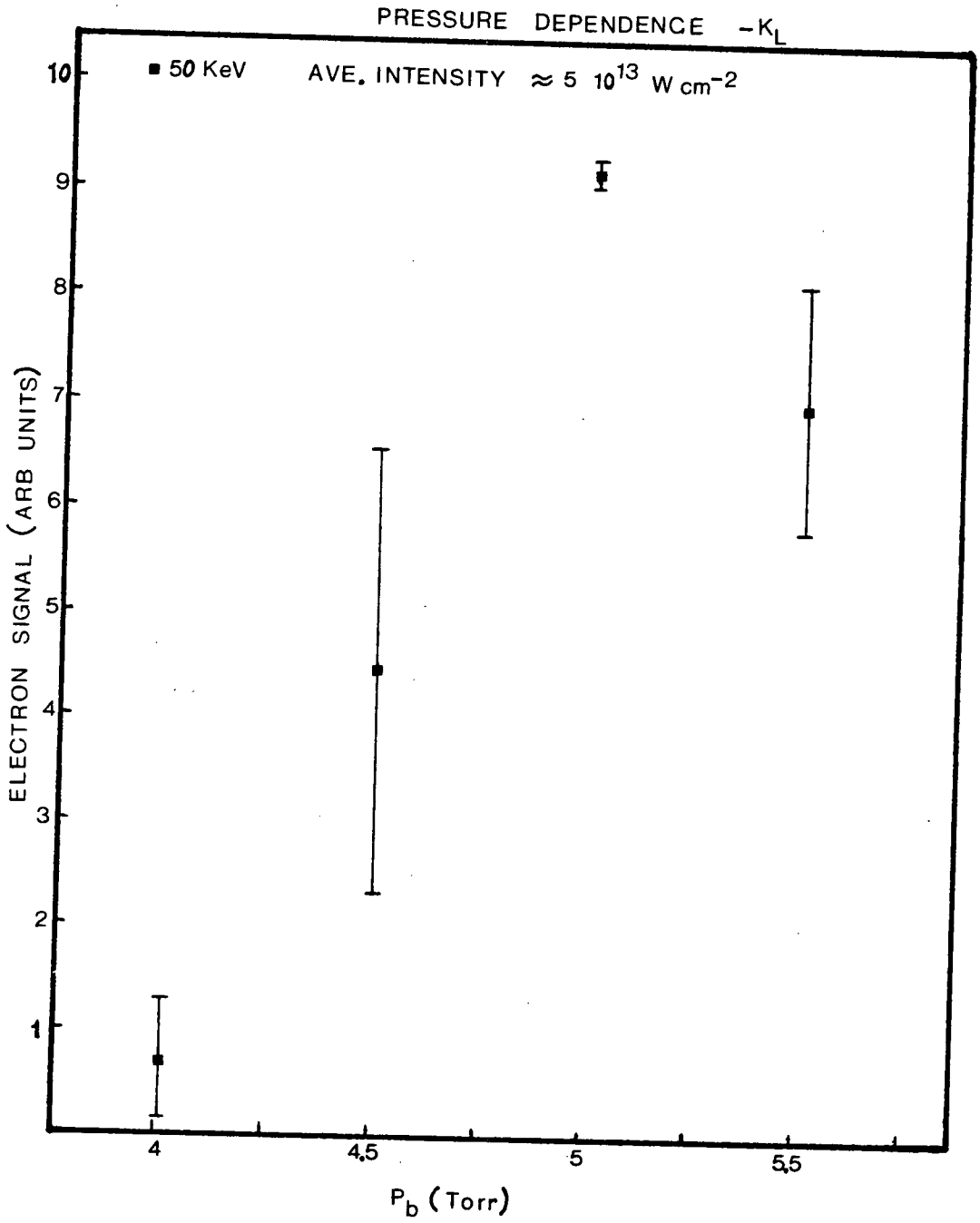
PRESSURE DEPENDENCE $-K_L$
■ 50 KeV
AVE. INTENSITY ≈ 5 10^{13} W cm^{-2}
ELECTRON SIGNAL (ARB UNITS)
10
9
8
7
6
5
4
3
2
1
4
4.5
5
5.5
P_b (Torr)

Figure IV-2

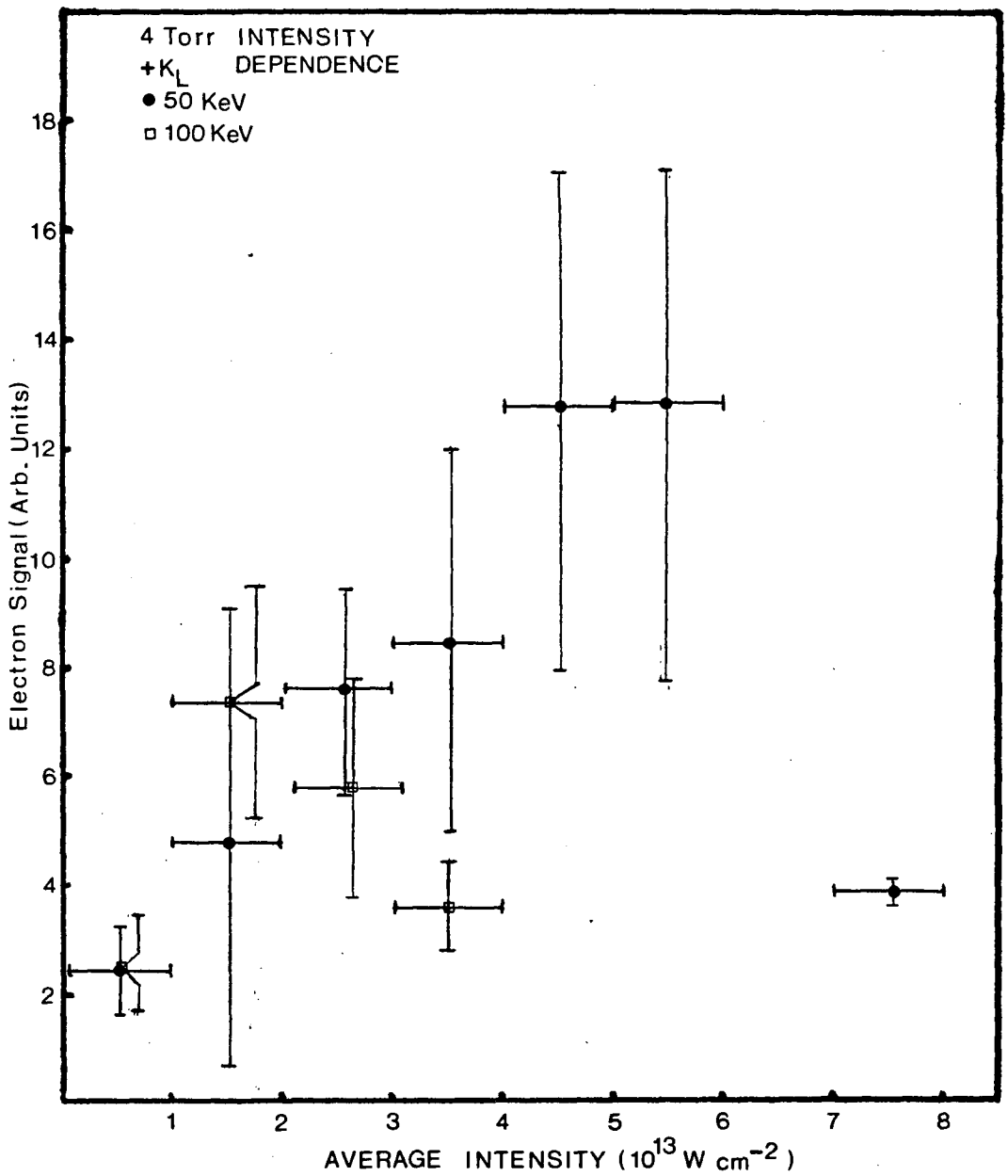
4 Torr INTENSITY
+K_L DEPENDENCE
● 50 KeV
□ 100 KeV
Electron Signal (Arb. Units)
AVERAGE INTENSITY (10^13 W cm^-2)
2
4
6
8
10
12
14
16
18
1
2
3
4
5
6
7
8

Figure IV-3

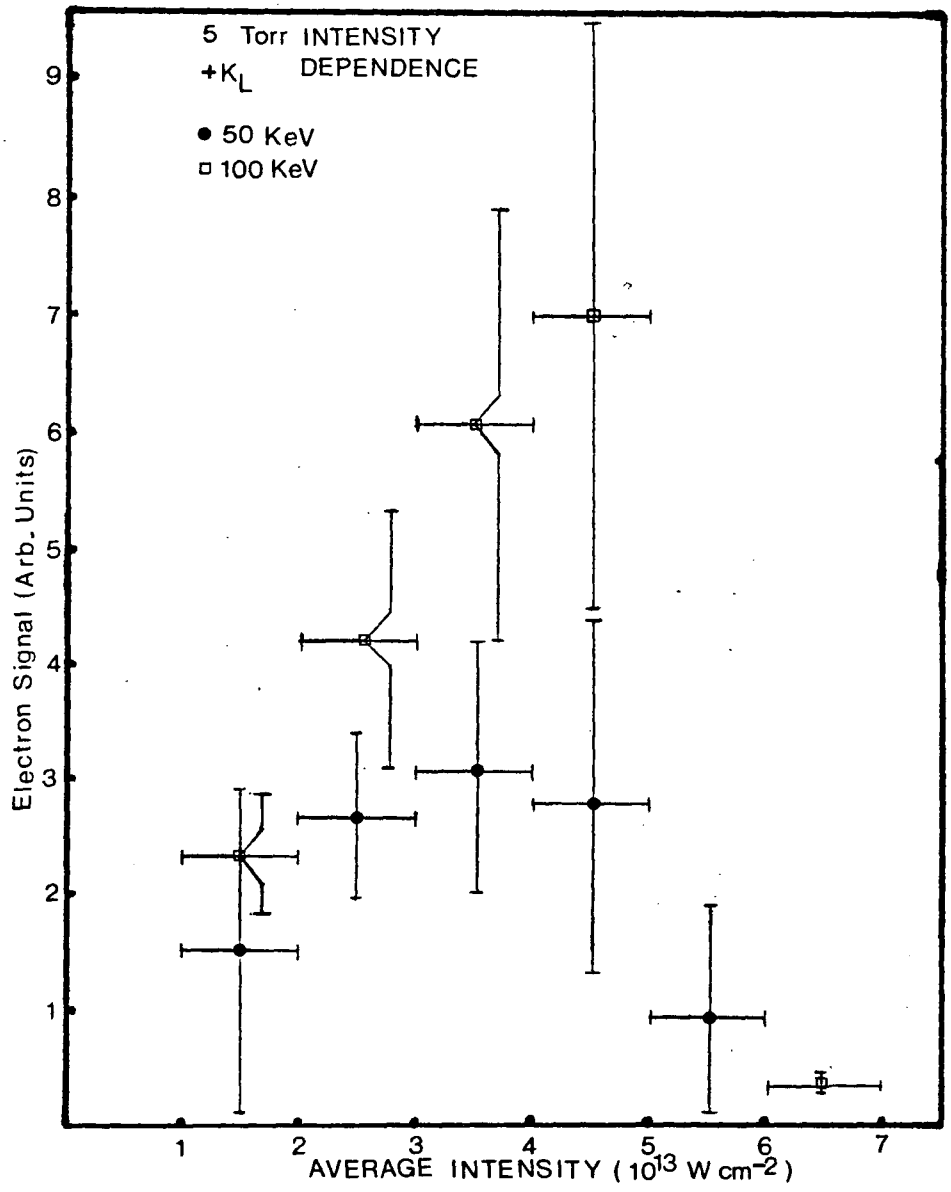
5 Torr INTENSITY
+K_L DEPENDENCE
● 50 KeV
□ 100 KeV
Electron Signal (Arb. Units)
AVERAGE INTENSITY (10^13 W cm^-2)
1
2
3
4
5
6
7
8
9

Figure IV-4

Torr jet, the 100 keV signal is on average smaller than the 50 keV signal whereas in the 5 Torr jet the 100 keV signal is 1.5 to 2 times as big as the 50 keV signal. This would seem to imply that for the 4 Torr jet there is a lower κT .

From the size of the signal one can attempt to estimate the numbers of fast electrons detected. To do this one must start with the signal and work backwards to the scintillator. Converting the voltage signal (100 mV) to a current signal by dividing by 50 ohms and integrating the current signal over time (10 ns fwhm) the total charge ($2\ 10^{-11}$ C) generated is found. Converting the charge to the number of electrons into the scope through division by the gain of photomultiplier ($4.8\ 10^{5}$) the number of photoelectrons emitted (250) is estimated. Dividing by the quantum efficiency of the photocathode (.2) the number of photons incident (1250) is found. Further correcting for losses at interfaces (7%/interface x 3) and in the optical fiber (85%) and for light emission in scintillator which does not get into optical fibers (4π/acceptance angle=5.5) , multiplying by the ratio of the energy of typical scintillator photon (3eV) to the energy of incident electron (50 keV) and finally dividing by the fraction of the incident energy ultimately emitted as visible light by the scintillator (assumed 1) one arrives at the number of electrons incident on the scintillator. For a 100 mV signal and 50 keV electrons incident the number arrived at is small , approximately 1 to 10 electrons. Since some signals are the equivalent (through N.D. Filters and non-linear response of photomultiplier) to 70 volts this means approximately 1000 electrons have reached the scintillator. This corresponds to

roughly 3 10^5 electrons sr^{-1} at 50 keV when divided by the solid angle.

Another piece of data analyzed was the percentage of shots where no (or very few electrons) were observed. This confirmed both the pressure and the intensity observations (see Fig IV-5): the lower the background pressure the less likely electrons will be observed and a dip at 4 10^{13} Wcm^{-2} confirming that it will be most likely to see electrons at this intensity.

In the process of calibrating the fibers for the OMA ,a few shots were taken with the foil-scintillator combination placed in the plane perpendicular to E_o of the laser. The shots indicated that the total flux of xrays and electrons was peaked in the backwards direction. The scintillators were located at 153,140,128 and 117 degrees to $+k_L$. This suggests the electron production is not isotropic, but peaked in the backwards (and presumably) forwards directions. The detailed angular variation was not actively pursued in this work, but has been reported elsewhere (Meyer et al., 1983).

Distribution Function

The four channel spectrometer confirms that a Maxwellian distribution fit is acceptable in the range 40 - 300 keV . The κT fitted is 121 keV (see Fig IV-6). The error in κT is estimated at 25%.

The signals from the OMA were corrected for relative channel response,energy loss in the foil and electron number

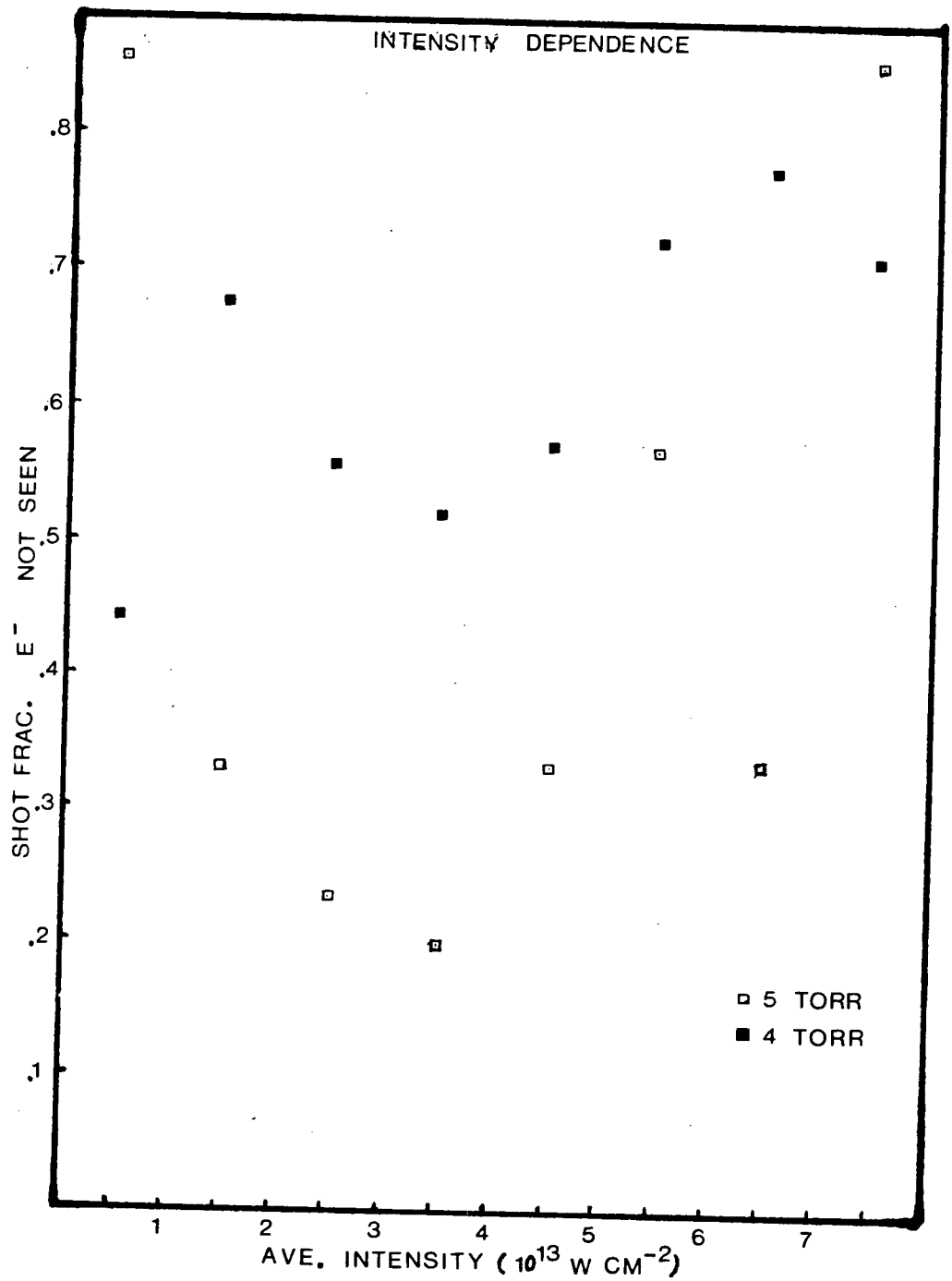
INTENSITY DEPENDENCE
SHOT FRAC. E⁻ NOT SEEN
.8
.7
.6
.5
.4
.3
.2
.1
1
2
3
4
5
6
7
AVE. INTENSITY (10^13 W CM^-2)
5 TORR
4 TORR

Figure IV-5

attenuation in the foil and were normalized for different incident energies. The results were fitted by a function of the form

$$f(\xi)=A\sqrt{(\xi)}\exp(-(\xi)/\kappa T) \qquad \text{(Fit 1)}$$

κT was found to be 121 keV. The 4 channel system was less sensitive than the one channel system. This is due to poorer quality optical fiber, smaller scintillator area (and smaller optical fiber area) and a possibly less tightly focused spectrometer.

A few words of caution must be expressed about the interpretation of the fit above. The fit was made since other experiments (Joshi et al.,1981; Ebrahim et al.,1981; Berger et al.,1983) have shown that such a fit will work. No underlying assumptions about the reason for the fit must be made . To further emphasize the point another fit

$$f(\xi)=A\exp(-B(\sqrt{\xi}-\sqrt{C})(\sqrt{\xi}-\sqrt{C})) \qquad \text{(Fit 2)}$$

was tried. C was 82 keV and B^{-1} was 26 keV. The fit is also good. Many more data points over a much wider energy range and with much smaller error bars must be used to resolve the difference.

The conclusions are that SRS electrons are produced quite efficiently produced in the .25 n_{CR} region of the plasma and the expected temperature based upon the simple SRS theory of the absolute instability at the .25 n_{CR} region is in good agreement with the experimental result.

ELECTRON ENERGY DISTRIBUTION

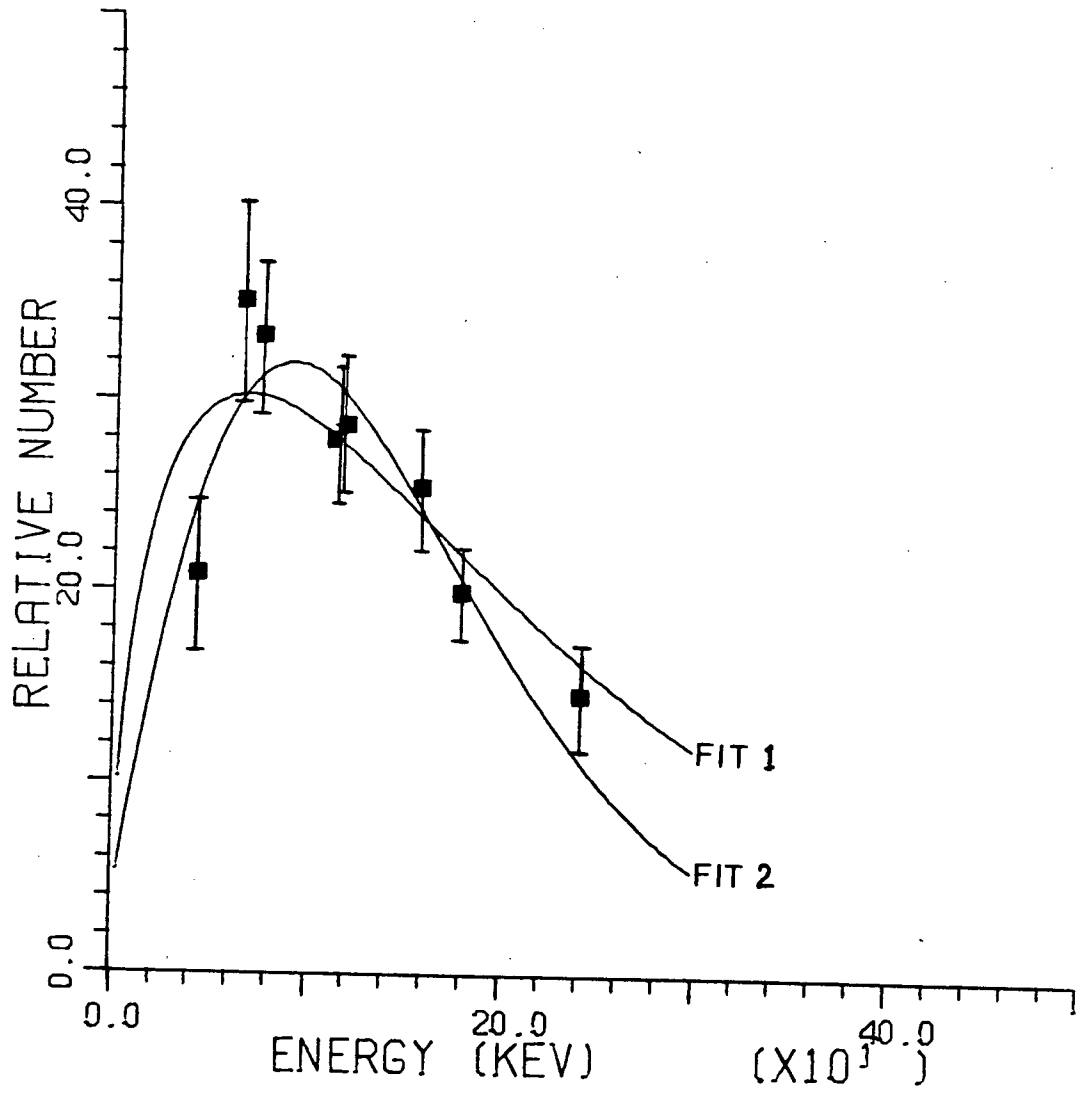

Figure IV-6

CHAPTER 5 INTERFEROMETRY

The results of chapter 4 raised some interesting points which require further study. The pressure dependence of the number of electrons may be due to the plasma density changing with changing background pressure. The intensity dependence may be due to small scale changes in the density . These small scale changes include modification of the scale length at .25 n_{CR} and will affect beam refraction in the plasma. It seems that a detailed investigation of the plasma density as a function of time ,space and incident laser energy must be undertaken. Interferometry with a short pulsed laser would be the most efficient way of accomplishing this objective. From the resulting interferograms a great deal of information can be extracted. The following can be given as functions of time,space and incident laser energy : plasma volume,total electron number, density,scale length and refraction effects.

The probe used for interferometry was a 80 ps ruby laser (wavelength 694.3 nm). A Jamin interferometer (Born and Wolf) was set up by B.Hilko and H.Houtman. And the plasma was probed. The interference fringes were recorded on Polaroid film and selected ones were photographically enlarged and digitized. The data was then analyzed by computer (see Appendix 1) and the results were plotted (see figures V-1 to V-5). The .25 n_{CR} line is emphasized.

General Results

The feature which is most striking is the existence of

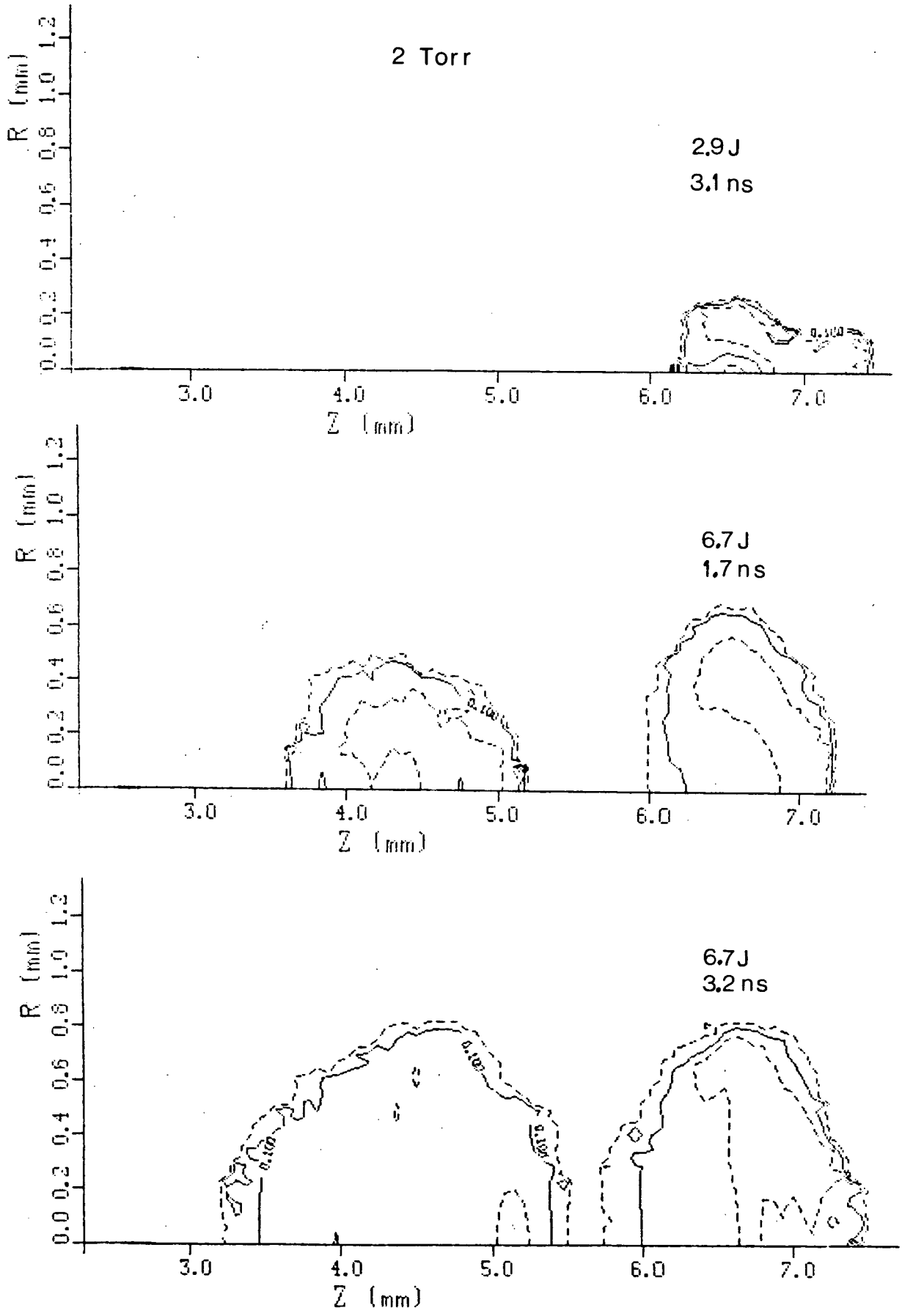
2 Torr
2.9 J
3.1 ns
6.7 J
1.7 ns
6.7 J
3.2 ns
R (mm)
Z (mm)
0.0
0.2
0.4
0.6
0.8
1.0
1.2
3.0
4.0
5.0
6.0
7.0

Figure V-1

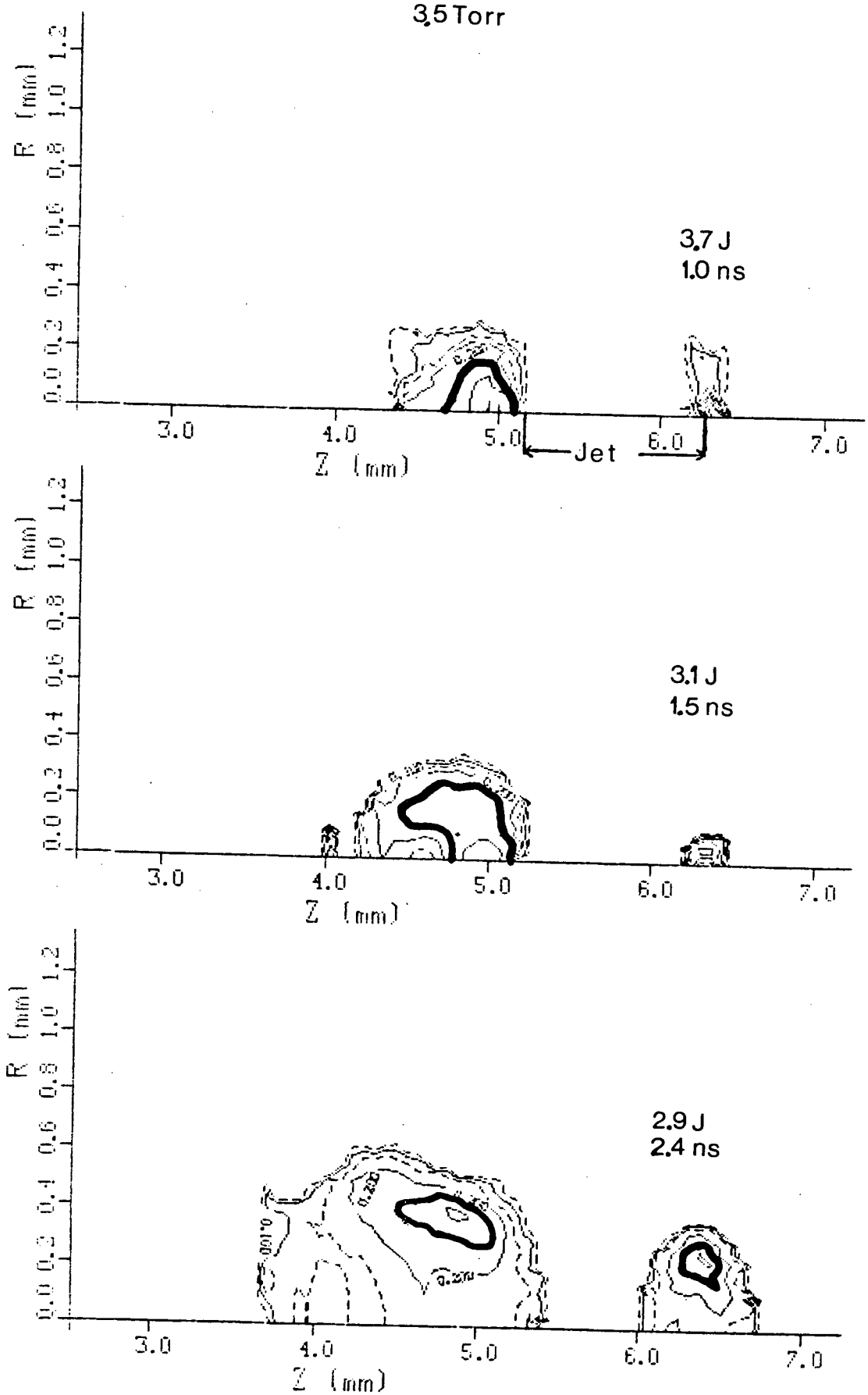
3.5 Torr
R (mm)
0.0 0.2 0.4 0.6 0.8 1.0 1.2
3.7 J
1.0 ns
3.0 4.0 5.0 6.0 7.0
Z (mm)
Jet
3.1 J
1.5 ns
2.9 J
2.4 ns

Figure V-2

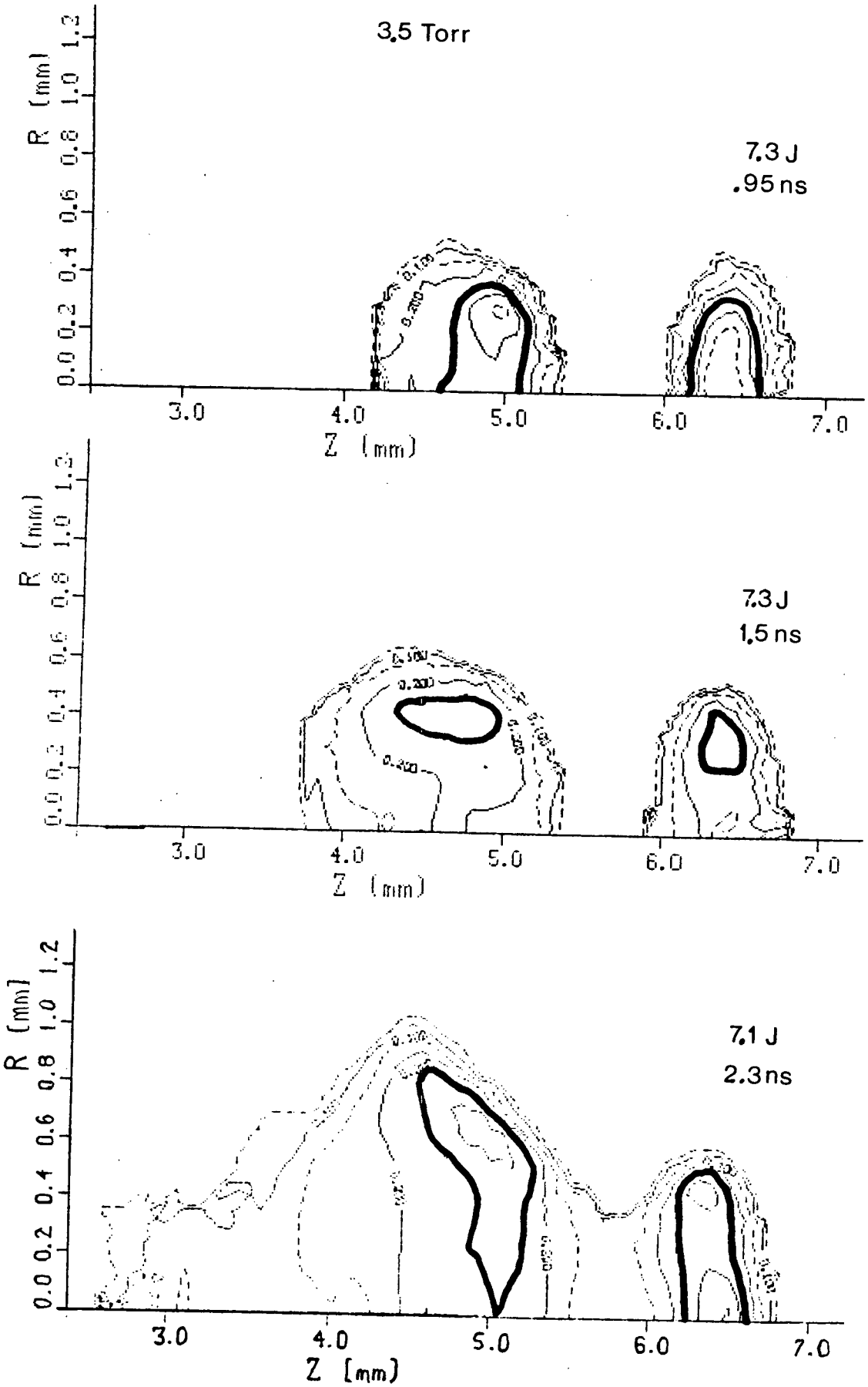
3.5 Torr
7.3 J
.95 ns
7.3 J
1.5 ns
7.1 J
2.3 ns
R (mm)
Z (mm)
0.0
0.2
0.4
0.6
0.8
1.0
1.2
3.0
4.0
5.0
6.0
7.0

Figure V-3

5 Torr

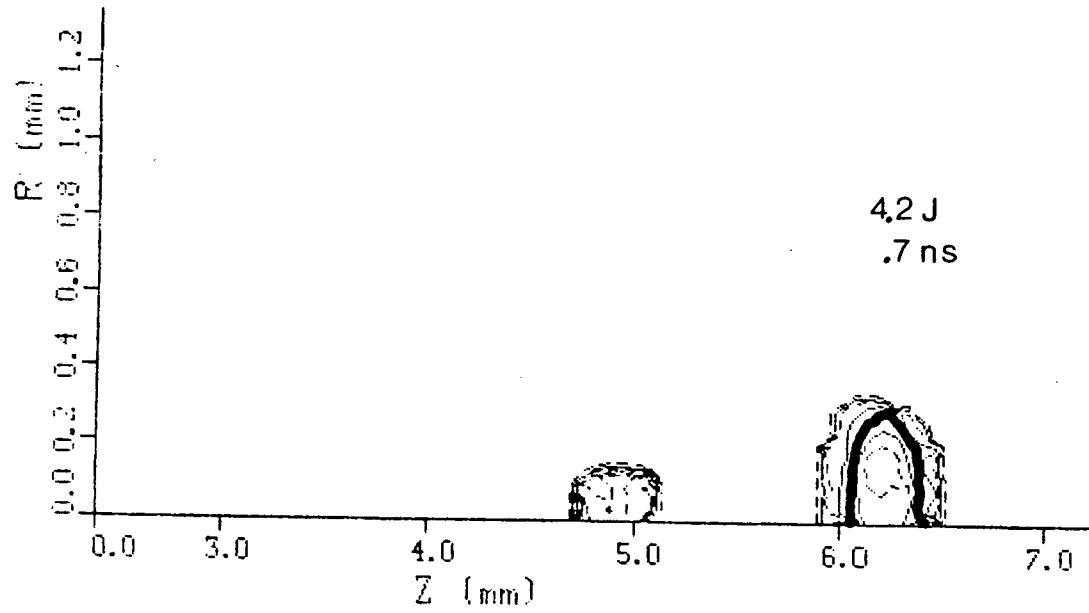

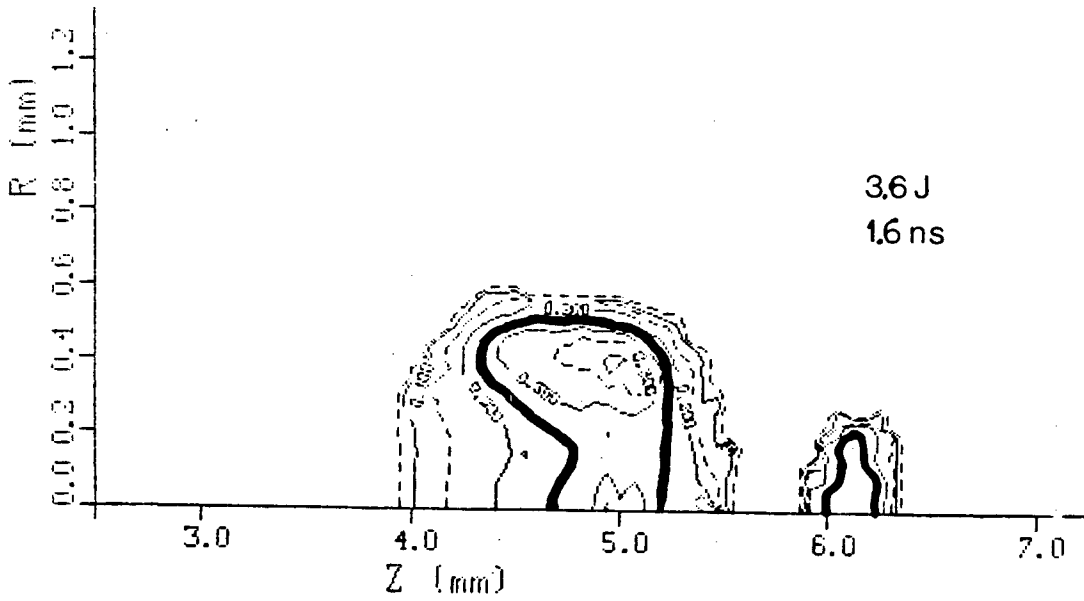

Figure V-4

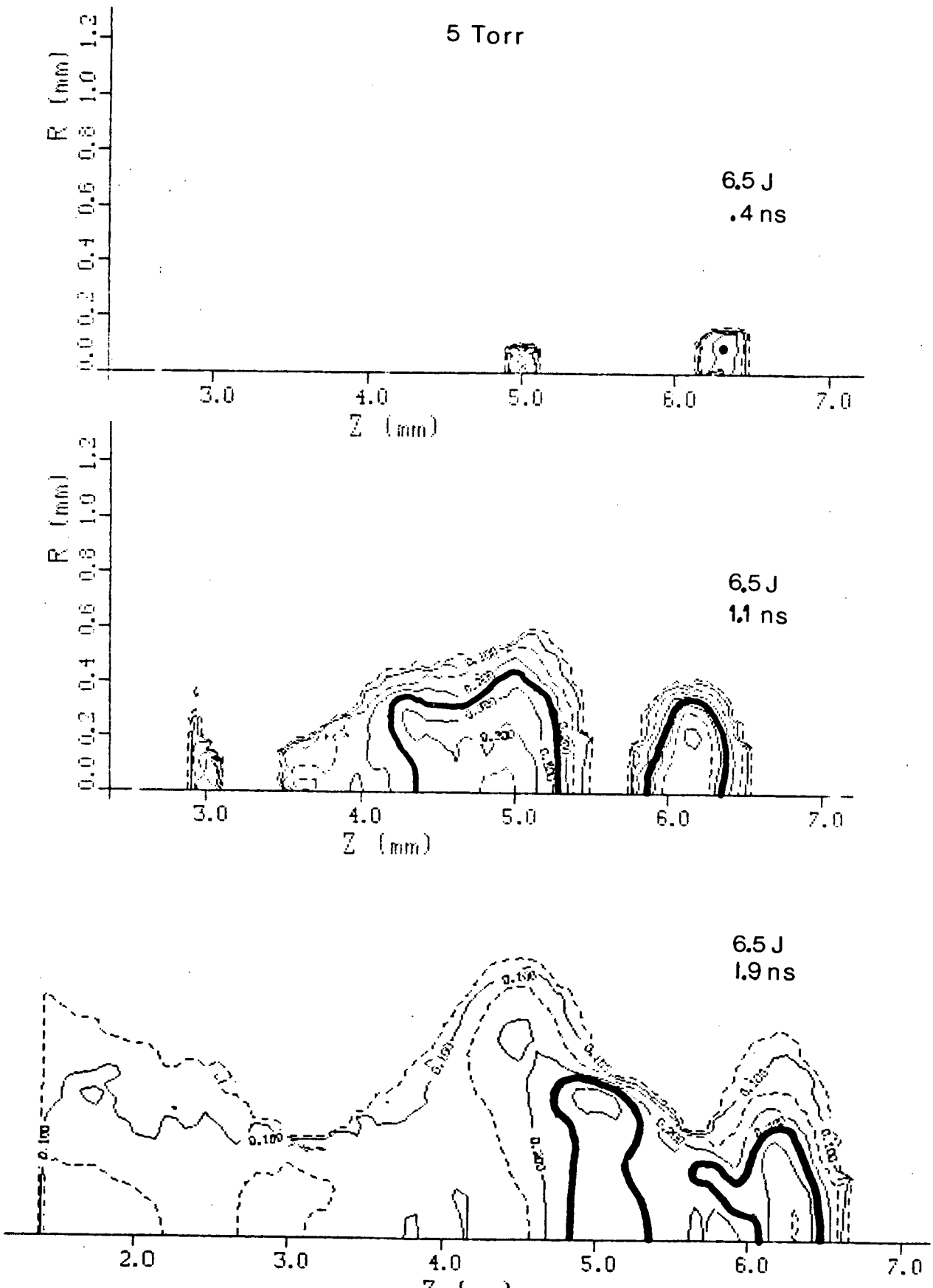

Figure V-5

three islands of plasma. Initially the island located at the rear edge of the gas jet is formed. The next island to appear is the middle one located at the front edge of the jet . This island appears less than 200 ps after the first. The final island appears in front of the jet and could be due to breakdown in the 5 Torr background gas. This is surprising since the calculated maximum density is $3.5\ 10^{17}\ cm^{-3}$. Contamination by nitrogen from the gas jet is possible since the jet will have been on for 7 ms before the laser pulse reaches it. It is more probable that expansion or blow-off of plasma from the middle island is the cause of the front island. It is interesting to note that while the density in the front plasma is high it is not as high as in the clumps located at the gas jet proper. These islands expand with time and eventually merge. After a few ns the plasma appears toroidal with the region of maximum density moving away from the axis.

Large Scale Results

The absolute number of electrons present in the entire plasma was calculated by merely integrating (via computer) the density over the volume :

$$N= \iint n(r)2\pi r\, dr\, dz$$

. The number calculated can be roughly estimated by using a plasma volume $=\pi r^2 l$ multiplied by the product of the molecular density and the Z of nitrogen. This yields an estimate of order 10^{15} to 10^{16} which agrees with the numbers computed.

The expansion velocity of the plasma was also examined. This is done by following a contour line as the plasma expands.

The total plasma volume itself was also calculated.

$$V = \iint 2\pi r \, dr \, dz$$

The results of the gross analysis of the plasma are in Fig V-6.

The expansion velocity is easily determined by finding the slope of the curves. What was plotted was the contour position at a fixed Z vs time. The general result indicates that the plasma expands at about few times 10^7 cm s^{-1} . The velocity measured depends upon several factors. The incident energy is important because as more laser energy is applied the plasma expands faster. The expansion rate also depends upon which contour one picks and which part of the plasma the contour is found.

The bulk plasma electron density distribution was also calculated. This distribution indicates the density regimes where the electrons in the plasma are to be found. Further the average density was also found by dividing the total number of electrons by the total plasma volume. This distribution is a convenient way of showing that at early times the density regime where the maximum number of electrons appear is lower for the lower Torr jets. At later times the distribution changes. This happens because the electrons are being moved into higher density regimes. Since the number of electrons is presumably fixed this means that electrons are being moved from lower density regimes . The distribution thus gains at the high end

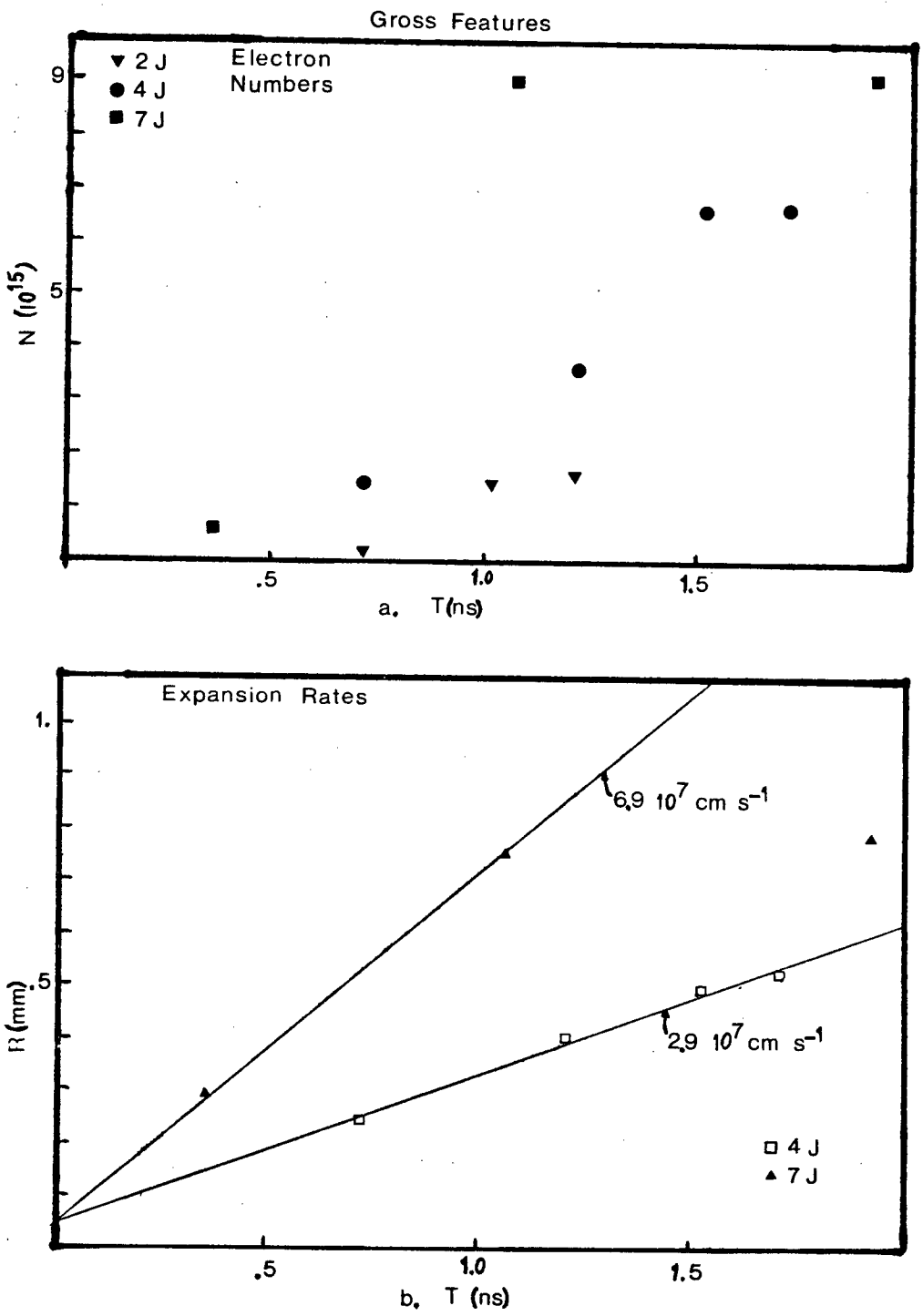
Gross Features
2 J
4 J
7 J
Electron
Numbers
9
5
N (10^{15})
.5
1.0
1.5
a. T(ns)
Expansion Rates
1.
.5
R(mm)
6.9 10^7 cm s^{-1}
2.9 10^7 cm s^{-1}
4 J
7 J
.5
1.0
1.5
b. T (ns)

Figure V-6

that this is happening.

The gross features reveal some not unexpected results. As more laser energy is applied to the plasma the greater is the rate at which the number of electrons grows . As more laser energy is applied the earlier the plasma appears . At any given time (early in the laser pulse) there are more electrons at the higher energies . There also appears to be a 'saturation' as the number of electrons appears to level off at later times.

Fine Scale Results

On a finer scale more detail can be measured. Caution must be used since small details are obscured by errors in digitizing and computational artifacts generated by imposing a 'mesh' (rectangular coordinate system) onto the interferograms. Some of this is compensated for by using a smoothing routine in the analysis. The main assumption of cylindrical symmetry (in order to do the Abel inversion) is also violated in some of the later interferograms.

Ray tracing was performed by J.E.Bernard. The results obtained (eg Fig V-8) indicate that the plasma refracts the laser away from the rear plasma. Also in the process of refraction the laser spreads out, lowering the intensity in the plasma.

One can estimate the density scale length in the plasma. In particular L can be found near the .25 n_{CR} layer. L is defined as

Bulk Plasma Electron Density Distribution

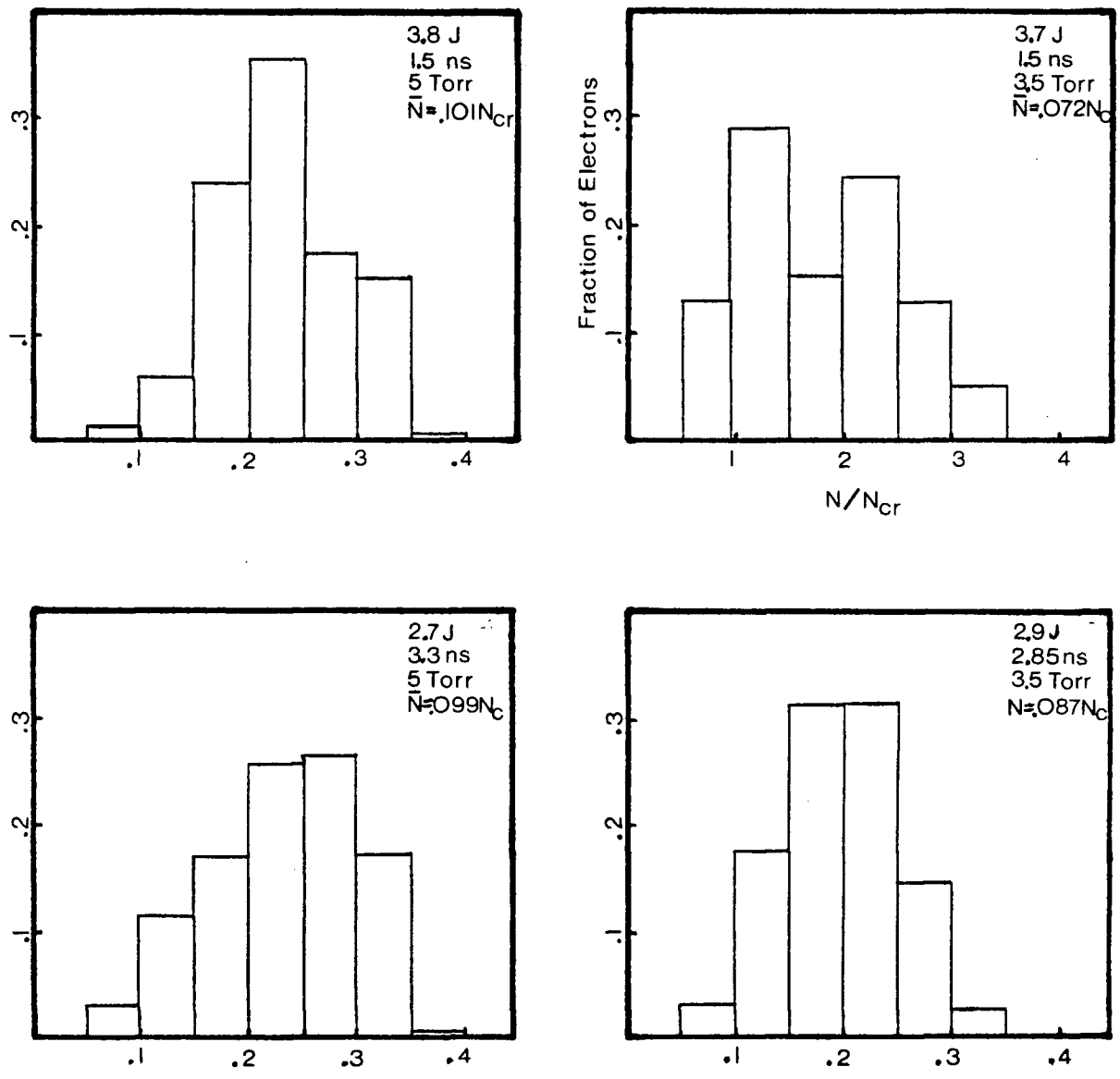

Figure V-7

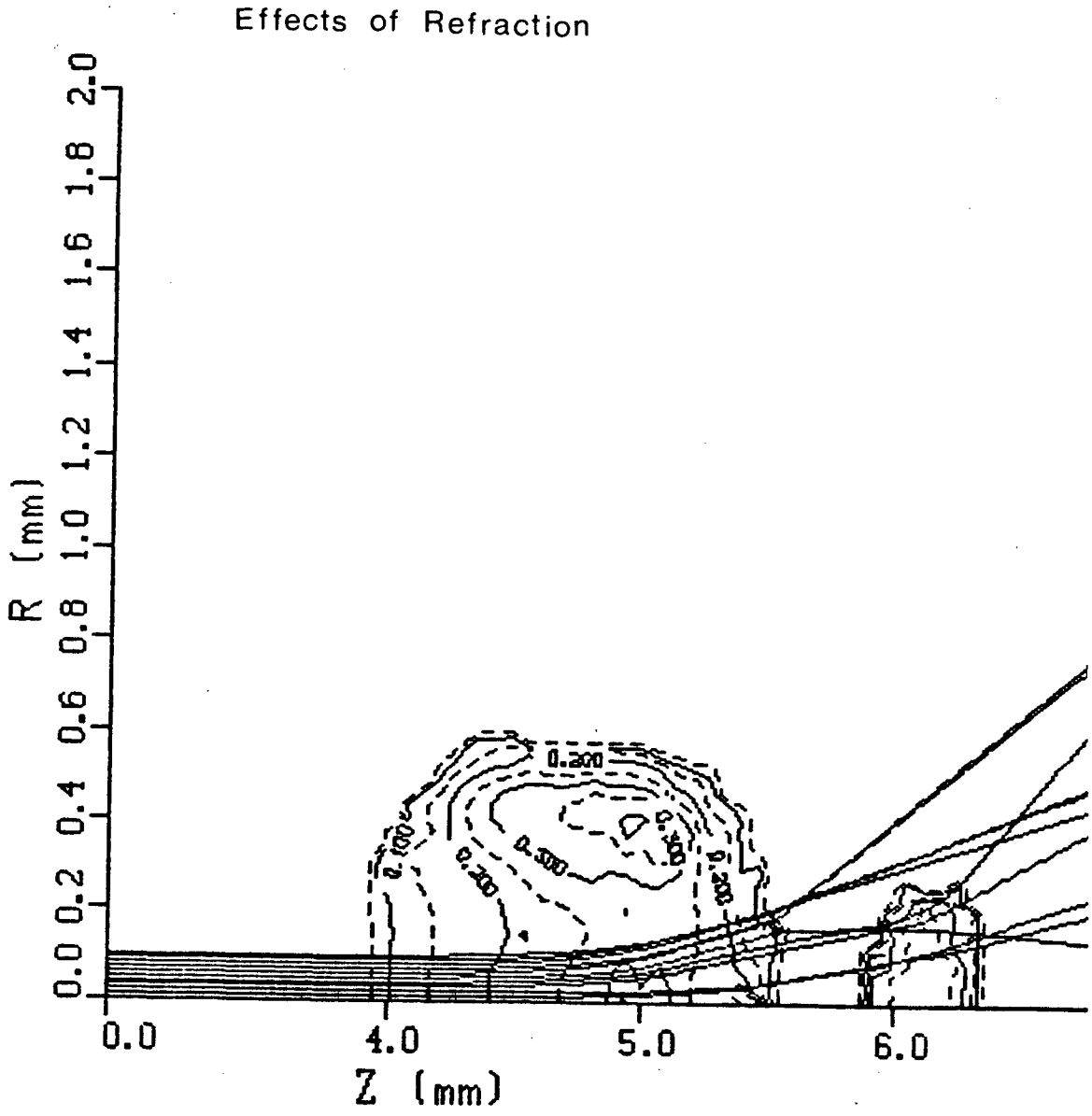
Effects of Refraction
R (mm)
0.0
0.2
0.4
0.6
0.8
1.0
1.2
1.4
1.6
1.8
2.0
0.200
0.100
0.300
0.400
0.0
4.0
5.0
6.0
Z (mm)

Figure V-8

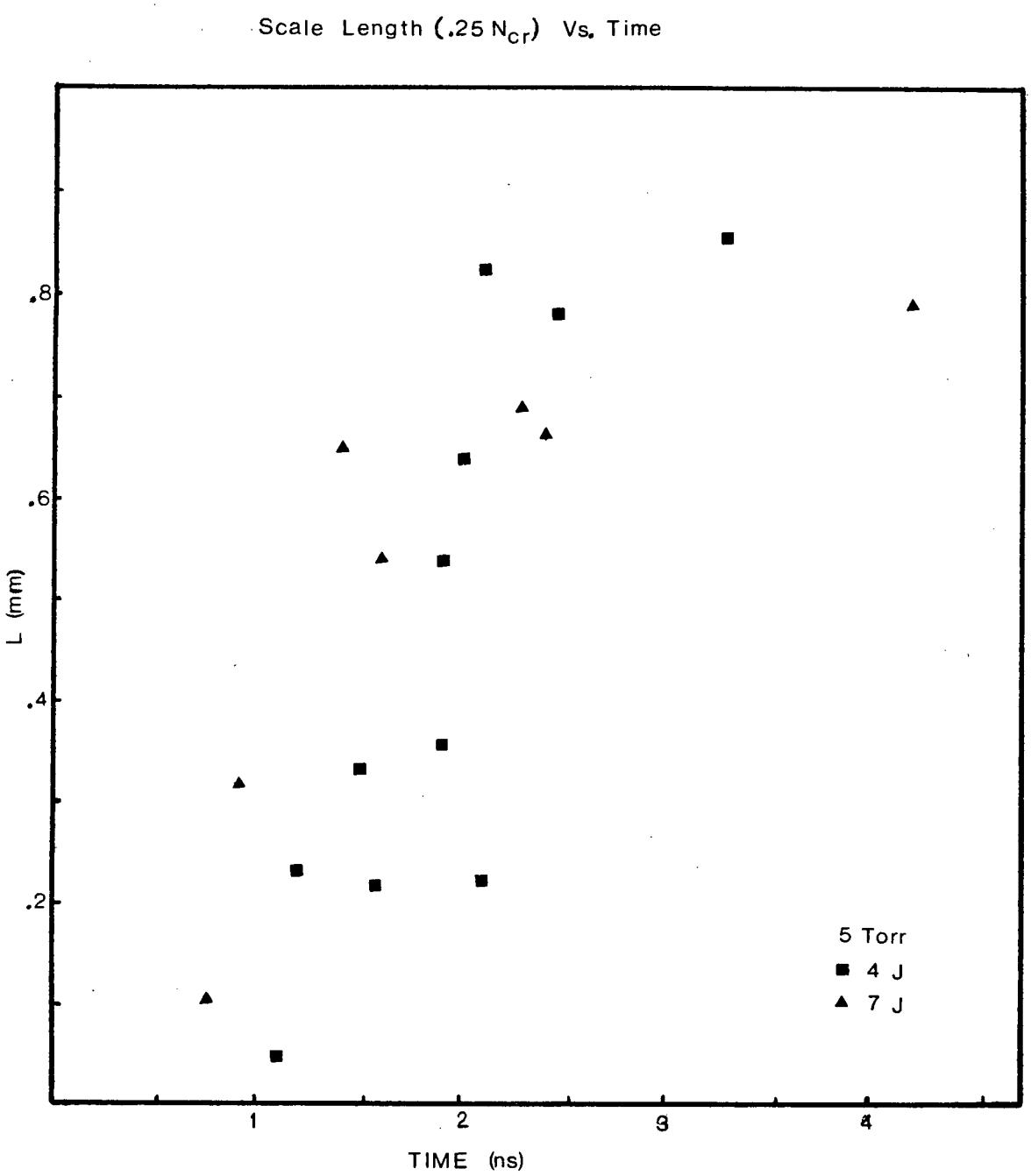

Figure V-9

$$L = 1/(1/n \ \ dn/dx)$$

. L is plotted in Fig V-9 as a function of time and energy. No distinct evidence is seen for scale length modification but the tendency is for the high power scale lengths to grow slightly slower and to not reach the maximum low power scale lengths. This could possibly be assigned to pondermotive forces which decrease the hydrodynamic expansion that is causing the scale length to increase.

CHAPTER 6 DISCUSSION AND CONCLUSIONS

The results of chapter 4 and chapter 5 will now be discussed. The conclusions will also be reviewed.

Pressure Dependence

In chapter 4 it was noted that the electron signal increases dramatically as the background pressure was increased. Since it is calculated that the maximum molecular density is proportional to the reservoir pressure it is reasonable to expect that the spatially and temporally averaged plasma density will be lower for the lower Torr jets. A comparison of the 2 Torr and 5 Torr jets clearly indicate this and is confirmed by the bulk plasma electron distribution function. Since at lower densities the growth rate and the phase velocity are much lower one should expect the number of electrons to be lower for a fixed energy. The lowering of the phase energy will lower the 100 keV:50keV signal ratio. For example if the average density is $.2n_{CR}$ the phase energy is 39 keV. Assuming that the fast electron distribution is Maxwellian , the signal ratio should be $100/50*\sqrt{(100/50)}\exp(-50/39)=.8$ whereas at $.25n_{CR}$ the ratio should be $100/50*\sqrt{(100/50)}\exp(-50/115)=1.8$. This is what is observed for the 4 Torr and 5 Torr results. It should be noted that for lower densities the k of the EPW is longer. This will increase the Landau damping and thus the waves will decay sooner. Also SRS is convective for lower densities and the growth rate is lower than in the absolute case.

Intensity Dependence

The absolute number of fast electrons generated by SRS is an important number. If the total number is very small then their relative importance in preheating a laser fusion target becomes negligible. In chapter 4 it was shown one could use an electron energy distribution fitted by

$$N(\xi)=C\sqrt{\xi}\exp(-\xi/\kappa T) \quad (\text{C is for normalization})$$

where $\kappa T=121$ keV. In chapter 3 the energy resolution of MK II was noted at +-15%. An estimate of the total fraction of the distribution entering the scintillator can be made by integrating over the distribution

$$N/N_o=4/\sqrt{\pi}\int x^2\exp(-x^2)\,dx$$

$$x^2=.5mv^2/(\kappa T)$$

. At 100keV we find $N/N_o=.13$. The largest electron signal at this energy corresponds to at least 1000 electrons. The total number of electrons is thus greater than 10000. This number is a lower bound on the total number of fast electrons. This is due ,in part, to the conservative estimate of the absolute number of electrons done in chapter 3. No integration over the solid angle into which the electrons were emitted was performed (other than the obvious one of the spectrometer). One must also realize that the electrons that have reached the detector correspond to the most energetic electrons created. The electrons which have escaped from the plasma must have overcome large potential barriers u which could be up to 200 keV. The fast electrons escape the plasma; the more massive positive ions are left behind giving the plasma a positive charge and hence the plasma obtains a potential . The electrons that we see at

energy ξ must have had energy $\xi+U$ in the plasma. The overall effect of the potential is to reduce the number of electron seen by a factor $\exp(-u/\kappa T)$.

Some idea of the total energy carried by hot electrons can be derived from the Manley-Rowe relations. These relations can be thought of as follows. For n given incident photons, n decay scattered photons and n decay plasmons can be generated. Each photon or plasmon has energy $h/(2\pi)\omega$. The total energy in a particular form is $nh/(2\pi)\omega$. Hence the following relationship holds:

$$\xi_o/\omega_o = \xi_s/\omega_s = \xi_p/\omega_p$$

Thus the total possible energy available for hot electrons is $\xi_p = \omega_p \xi_s/\omega_s$. At .25 n_{CR} a maximum energy of $.5\xi_o$ could appear as fast electrons. This is an overestimate as it neglects the kinetic energy of the background plasma which will be raised by SRS. Computer simulations (Hiob and Barnard) indicate that approximately 25% of the incident energy should appear as fast electrons. At least .05% of the incident energy appears as fast electrons in our case . When one considers that approximately 70%+ of the incident energy is not trapped in the plasma (ie is transmitted , Brillouin backscattered and refracted) (Popil Ph.D Thesis 1984 ; Bernard Ph.D Thesis 1984) quite a considerable fraction of the absorbed energy has shown up as fast electrons. Fast electrons are consequently quite important and must be considered when designing laser fusion reactors.

The threshold for SRS is also important. The ideal laser fusion laser wavelength must be chosen so that there is very

good absorption (leading to high ablation pressures and to good compression) with no fast electron production. (The advantage of shorter wavelengths is that inverse bremsstrahlung absorption, a major heating mechanism,is proportional to λ^{-2}). Since the thresholds observed in this work (10^{13} Wcm^{-2}) are in good agreement with the theory the theories should work well in calculating the shorter wavelength thresholds. Hence, for .53 μm light intensities should be kept below $\sim 4\ 10^{15}$ Wcm^{-2} to prevent hot electron production.

Since it has been shown that fast electrons are produced one should ask oneself whether there is a limit to the number that can be produced. An extreme upper limit is set by the Manley- Rowe relations (above). Fortunately there are other mechanisms that saturate and quench SRS. Saturation is observed when the scattered SRS light level stops rising exponentially (as is should near threshold) and levels off at incident intensities well above threshold. Since the number of fast electrons detected is related to the amplitude of the underlying SRS plasma wave , a saturation and quenching of the electron signal indicates a corresponding saturation and quenching in SRS wave amplitude. It is therefore instructive to examine the mechanisms which are responsible for the saturation of SRS.

One saturation mechanism is particle trapping (Hiob and Barnard,1983) . The underlying plasma wave generated in the SRS interaction grows to such a large amplitude that an appreciable fraction of the electrons in the plasma are trapped in the electrostatic potential of the wave. The detection of fast

electrons is a necessary but not sufficient proof of this saturation mechanism. Non-linear Landau damping of any large amplitude plasma wave will also generate fast electrons.

Other mechanisms can saturate SRS before the instability has grown large enough to generate fast electrons. The electrostatic wave generated can subsequently decay into a daughter EPW and IA wave. Indeed Karttunen ,1980 claims '...that the Langmuir decay starts to dominate the stimulated Raman scattering even at very low levels of the Langmuir wave amplitude indicating a strong saturation effect on SRS except at extremely high temperatures'. By comparing the growth rates for the decay process and SRS we find for our case (κT=1keV, n=.25n_{CR}) that

$$\gamma_L/\gamma_{SRS} = 215\ E_{EPW}/E_o \quad .$$

Thus it is possible that this is a mechanism for the saturation of SRS at high intensities.

Another mechanism which can saturate SRS is scale length modification (Chen and Liu). The EPW generated by Raman scattering (and more importantly, by the two plasmon decay instability) cause a gradient in E^2. This gradient results in a force (the pondermotive force) which tends to move ions and electrons out of the region where the waves are being generated namely near .25n_{CR} . The result of this is to change an initially linear density ramp into a steep gradient at .25n_{CR} and a plateau at a lower density. The SRS is convective (growing in space only) for densities below .25 n_{CR} and is absolute (growing in space and time) only near .25n_{CR} . Thus

fast electrons will not be seen as SRS will shut down before the wave can trap a large number of electrons.

Other theories which predict saturation include the decay of the backscattered EM wave (Karttunnen and Salomaa,1979) and reflection front propagation (Kruer et al,1975). These will not be discussed here.

There can be other processes independent of the saturation mechanisms discussed above which can explain the disappearance of the electrons at high intensities. These must be discussed as our results are not predicted by any theory nor seen in other experiments. Two such processes can occur in our experiment.

Early refraction causes the laser intensity seen by the plasma at .25 n_{CR} layer decrease earlier for the high power shots. This happens since the plasma in front of the gas jet due to the ionization of the He background gas forms earlier for the high power shots and thus refraction of the laser can start earlier and the intensity drops below the threshold intensity early in the laser pulse . Although not shown on all the interferograms plotted the original interferograms show some evidence (eg blurring of fringes or very small fringe shifts) of breakdown in the background Helium gas. While the density is low (less than .1 n_{CR}) the long distances (greater than 3 mm) compensate and the net effect could be considerable refraction. A ray tracing calculation shows that this is a reasonable assumption (see Figure VI-1) . The density form assumed is shown in the figure and is independent of the Z coordinate. Early refraction is also supported by temporally resolved

transmission measurements (Bernard, Ph.D Thesis 1984). These show that as the incident laser intensity is increased the transmitted power through the f/5 exit lens decreases to zero earlier. In fact for the highest powers the transmission is over before the peak of the laser pulse has arrived. It is difficult to estimate the instantaneous power with refraction taken into account. A rough estimate can be obtained from the ray tracing where the radius containing the rays squared can used as a measure of the relative intensities. A modest 50% increase in radius will reduce the intensity by more than a factor of 2.

Secondly, rapid expansion could explain the disappearance of fast electrons. The plasma expands expands rapidly leaving a low density hole . This hole appears earlier for the high power shots and thus the bulk of the laser pulse will see an effectively lower density plasma. Thus sampling fixed energies will yield the same results as lowering the background pressure. Simulations done with CASTOR (which is a 2-D hydrodynamic code for laser plasma interactions) indicate that the blow-out does start very early into the pulse. This explanation is plausible only if the refraction hypothesis presented is wrong as the expansion hypothesis requires the laser to pass through the same focal volume for the low and high power shots. The Raman scattering must also occur late in the pulse ie when the dense plasma has actually blown out of the focal volume.

The above discussion is fine for general explanation of the intensity dependence, but detailed numerical analysis is

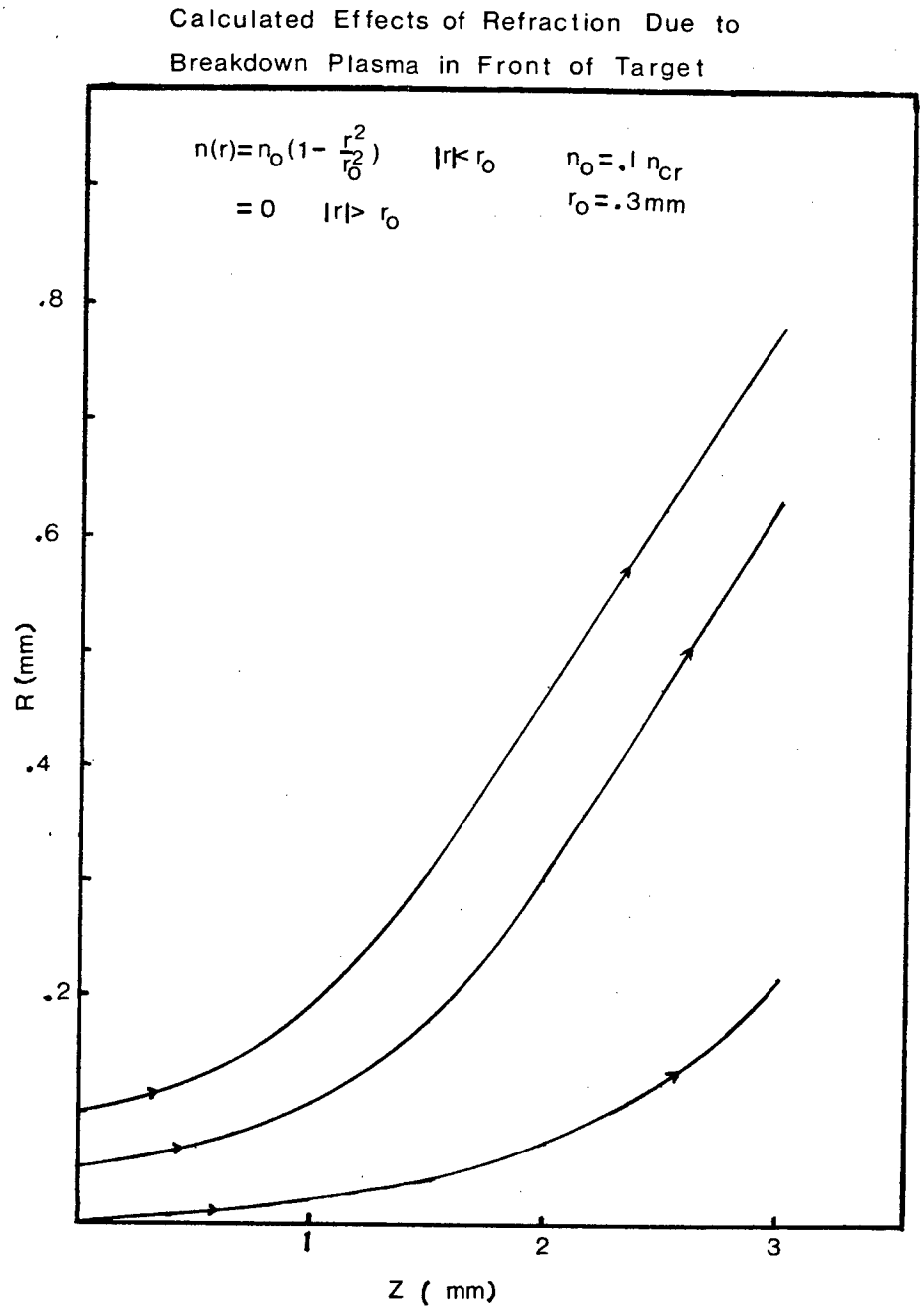
Calculated Effects of Refraction Due to
Breakdown Plasma in Front of Target
$n(r)=n_o(1-\frac{r^2}{r_o^2})$ $|r|<r_o$ $n_o=.1\ n_{cr}$
$=0$ $|r|>r_o$ $r_o=.3mm$
.8
.6
.4
.2
R (mm)
1
2
3
Z (mm)

Figure VI-1

difficult the theoretical thresholds are not unique, but rather are order of magnitude estimates and variations from theory to theory of two or three are quite possible. For example for L=300 μm and n=.25n_{CR} Kruer's theory predicts I_T=5 10^{13} Wcm^{-2} whereas Chen predicts I_T=1.58 10^{14} Wcm^{-2}. Since the experiments were performed very close to the calculated thresholds subtle variations in L or I could have dramatic effects on the electron signal. It is , however, very difficult to prove any of these possibilities without more experiments. To see scale length modification the density variations must be known quite accurately with small error bars and for early times when the radius of the plasma is less than 200 μm. While interferometry is capable of doing this (in principle) the amount of data analysis can become rather arduous. This is why the digitizing was done and the computer program was written. The gain in the ease of analysis is balanced by a (practical) decrease in accuracy. Refraction calculations depend on the quality of the interferometric analysis as the ray tracing is extremely sensitive to small rapid changes in the density. Only the most general trends can be extracted from the ray tracing.

Energy Distribution Function

The energy distribution function for the fast electrons will now be discussed. One function which fits the data well is the one would expect if a Maxwellian distribution resulted. As noted earlier however the data are insufficient to claim that a Maxwellian is the best fit. If it assumed that it is a κT of 121 keV is obtained. This is very close to the phase energy for

an Raman EPW generated at densities near .25 ncr (=115 keV ,Chapter 2).

A Maxwellian distribution is the distribution expected if the fast electrons have come to equilibrium among themselves (thermalized). The time for thermalization has been calculated and we found the time necessary is much longer than the laser pulse time. It does not seem possible to find a physical mechanism for thermalization. As noted earlier other fits are possible. For example in chapter 4 Fit 2 was tried. The physical basis for attempting this fit was the assumption that we had a beam of electrons with some drift velocity and some Gaussian shaped spread about this drift velocity.

The essential results of this work are as follows. Fast electrons are generated quite efficiently by SRS whenever a significant amount of .25 n_{CR} plasma is present. The fluxes generated are greater than 3 10^6 sr^{-1} from the total number of electrons in the <u>focal</u> volume of 10^{12} . The energies of these electrons are consistant with a Maxwellian type distribution at a κT=121 keV. The most probable energy is in good agreement with that expected from the simple theory of SRS. The effects of refraction are important for the production of electrons when the incident intensity is near the threshold intensity. Further work must be done to completely understand the physics of the time evolution of temperature, density and local intensity in the laser plasma interaction studied in this work and their effect on the number of fast electrons.

APPENDIX 1

INTERPRETATION OF INTERFEROGRAMS:COMPUTER PROGRAM

A computer program was written which will interpret digitized interferograms. A listing of the program follows.

In order to understand the computer program some background information on interferometry must be presented. Interferometry is based upon the interference of two beams E1 (the reference beam) and E2 (the probe beam). Since both beams in our case have a common source (a ruby laser) the interference pattern will depend only on the phase difference between them. In the absence of plasma the phase difference is caused by different path lengths. This situation is characterised by evenly spaced straight fringes. If a plasma is present the phase difference will depend on the optical path length in the plasma as the plasma has an index of refraction

$$\mu = \sqrt{(1-n(r)/n_{CR\ RUBY})}$$

The phase difference in a cylindrical symmetric plasma is given by

$$\Delta = 2\pi/\lambda \left(\int \mu(r)\, dx - \int \mu_o\, dx \right)$$

where μ_o is the vacuum index of refraction. Following Fan and Squire one makes a change of variables to get

$$\Delta(y) = 2\pi/\lambda \int \mu^* 2r \,/\sqrt{(r^2-y^2)}\, dr$$

Abel inversion is performed to find $\mu^*(r)$ from $\Delta(y)$ (for the geometry see the figure).

The computer program does the analysis of the interferograms. The effects of the various subroutines are

outlined schematically in the figure. The center of the fringe is calculated using the first moment of the fringe shift.

$$y_{CENTER} = \sum(\Delta(i)*y(i))/ \sum(\Delta(i))$$

The radius is calculated by moving out from the center until the fringe shift equidistant from the center is below the error amount. The phase shift at radius r is found by averaging the phase shifts at r above and r below the center. The phase shift as a function of y is then Abel unfolded to provide n(r) using the computer program of Fan and Squire. A basic approximation used is that

$$\mu^* = \sqrt{(1-n/n_{CR})} - 1 \text{ is about } n/(2*n_{CR})$$

The program is straightforward to use. One digitizes a photograph so that an undeviated fringe follows a vertical line. All fringes should start evenly and end evenly with a margin around the fringes. The beginning and end of a fringe should lie on the undeviated part of the fringe.

At the beginning of the data file certain parameters should be specified. These are : (1) photo number (2) position of minimum and maximum y (chosen so that there is a small margin around the fringes) (3) number of evenly spaced slices between ymin and ymax (up to 150) , the number of fringes (up to 125) and the amount of smoothing n (averages 2n+1 points) (4) the spacing between fringes on the photograph and the actual spacing of fringes (magnification = photo spacing/actual spacing) (5) error (tolerance) in radians :below this level phase shifts are made zero and sign (+1 or -1) of the dominant fringe shift (shifts of opposite sign are made zero) . Before the data for

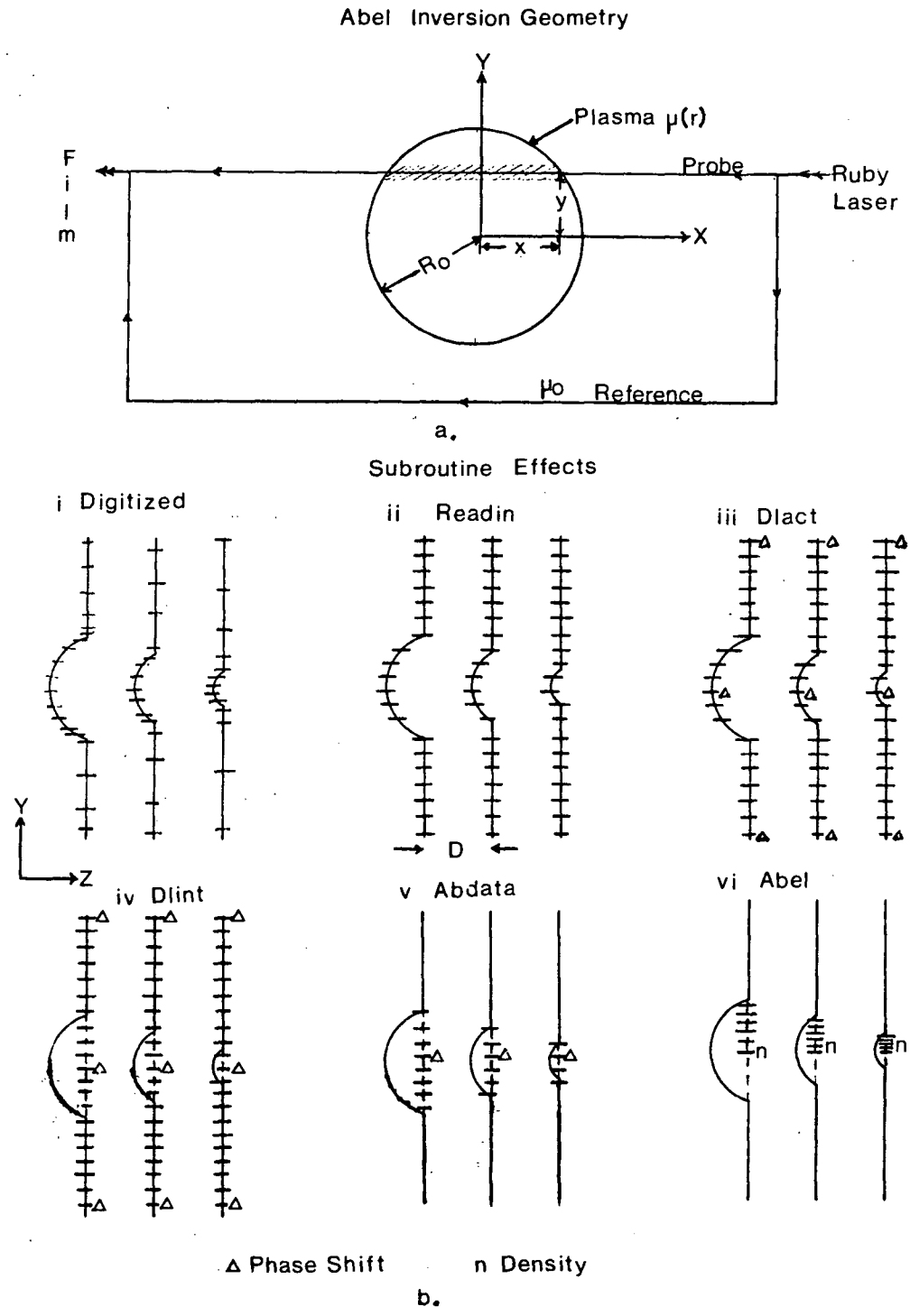
Abel Inversion Geometry
Y
Plasma μ(r)
Film
Probe
Ruby Laser
y
X
x
Ro
μo Reference
a.
Subroutine Effects
i Digitized
ii Readin
iii Dlact
Y
Z
D
iv Dlint
v Abdata
vi Abel
n
n
n
Δ Phase Shift
n Density
b.

Figure A-1

each fringe the number of the fringe and the number of points on the fringe should be specified. The points along the fringe do not have to be evenly spaced; the program does the interpolation to even spacing.

The amount of memory required to run program depends upon the size of the arrays . The program as listed required about 20K for the object code compiled under FORTRAN IV-H and the arrays require about 300K. The execution time required is generally under 5s CPU time on an AMDAHL 470 V-8 for an interferogram of 100 fringes and 90 slices per fringe.

```
      DIMENSION RAW(150,125), DELACT(150,125), DELINT(150,125),
     1          DELRAD(150,125), IRADS(1000)
      DIMENSION ROUT(1000), DENS(1000), XOUT(2500), YOUT(2500),
     1          ZOUT(2500)
      DIMENSION XT(2500), YT(2500), ZT(2500)
      LOGICAL FLAG(1000)
      DO 10 I = 1, 1000
   10 FLAG(I) = .TRUE.
      CALL READIN(RAW, NY, NFR, D, DELY, FRACT, SIGN, ERROR,
     1     YMAX, YO, NSMTH)
      WRITE (6,120)
      CALL DLACT(RAW, DELACT, NY, NFR, D)
      WRITE (6,120)
      CALL DLINT(RAW, DELACT, DELINT, NY, NFR, ERROR, D, SIGN,
     1     NSMTH)
      WRITE (6,120)
      CALL ABDATA(DELINT, NY, NFR, DELRAD, IRADS, FLAG, SIGN,
     1     ERROR)
      NFRMAX = NFR - 1
C COMPUTE NUMBER OF DATA POINTS TO BE USED IN PLOTTING PROGRAMS
      NOUT = 21
      NP = NFRMAX * NOUT
      WRITE (8,130) NP
      N = 0
      DO 50 IFRNO = 1, NFRMAX
C DO ABEL INVERSION WHERE POSSIBLE
        IF ( .NOT. FLAG(IFRNO)) GO TO 30
        NDS = IRADS(IFRNO) + 1
        WRITE (6,140) IFRNO
        CALL ABEL(DELRAD, NDS, IFRNO, ROUT, DENS, NOUT, D,
     1       DELY, FRACT)
C CREATE DATA ARRAYS FOR 3-D PLOTS
C   XOUT =  Z POSITION (DIRECTION LASER IS INCREASING FRINGE NO.)
C   YOUT =  RADIUS
C   ZOUT = DENSITY
        DO 20 II = 1, NOUT
          N = N + 1
          XOUT(N) = FLOAT(IFRNO) * FRACT
          YOUT(N) = ROUT(II)
   20   ZOUT(N) = DENS(II)
        GO TO 50
C IF NO FRINGE SHIFT ,PAD WITH ZEROS
   30   DO 40 J = 1, NOUT
          N = N + 1
          STEP = (YMAX - YO) / 2. / FLOAT(NOUT) * FRACT / D
          XOUT(N) = FLOAT(IFRNO) * FRACT
          YOUT(N) = (FLOAT(J) - 1.) * STEP
          ZOUT(N) = 0.000
   40   CONTINUE
   50 CONTINUE
C*****************************************
C REWRITE DATA IN 'PROPER' ORDER IE REVERSE THE Z DIRECTION
C THIS SECTION REMOVABLE IF FRINGES DIGITIZED CORRECTLY
C CHANGE Z COORDINATE
      N = 1
      DO 70 I = 1, NFRMAX
```

```
        DO 60 J = 1, NOUT
          XOUT(N) = FLOAT(119 - I) * FRACT
          N = N + 1
   60   CONTINUE
   70 CONTINUE
C REARRANGE
      N = 1
      DO 90 I = 1, NFRMAX
        DO 80 J = 1, NOUT
          XT(N) = XOUT(NP - I*NOUT + J)
          YT(N) = YOUT(NP - I*NOUT + J)
          ZT(N) = ZOUT(NP - I*NOUT + J)
          N = N + 1
   80   CONTINUE
   90 CONTINUE
C REWRITE
      DO 100 I = 1, NP
        XOUT(I) = XT(I)
        YOUT(I) = YT(I)
        ZOUT(I) = ZT(I)
  100 CONTINUE
C*********************************************
C WRITE 3-D PLOT DATA ON UNIT 8 (= SOME FILE)
      WRITE (8,150) (XOUT(I),YOUT(I),ZOUT(I),I=1,NP)
  110 STOP
  120 FORMAT (' ', ' ')
  130 FORMAT (I4)
  140 FORMAT (' ', ' RESULT FOR FRINGE NO', I4)
  150 FORMAT ((6(G10.4,2X)))
      END
C=============================================================
      SUBROUTINE READIN(RAW, NY, NFR, D, DELY, FRACT, SIGN,
     1           ERROR, YMAX, YOO, NSMTH)
C THIS PROGRAM IS TO DO INTERPOLATION ON DIGITIZER DATA
      DIMENSION Z(1000), Y(1000), RAW(150,125), IZ(1000),
     1          IY(1000)
C READIN ALL DATA RELEVANT TO THE PROGRAMS EXECUTION
      WRITE (8,100)
      READ (5,110) IPHOTO
      WRITE (8,110) IPHOTO
      WRITE (6,230) IPHOTO
      READ (5,120) YO, YMAX
      WRITE (6,130) YO, YMAX
      READ (5,140) NY, NFR, NSMTH
      WRITE (6,150) NY, NFR, NSMTH
      READ (5,160) D, FRACT
      WRITE (6,170) D, FRACT
      READ (5,180) ERROR, SIGN
      WRITE (6,190) ERROR, SIGN
C IPHOTO = PHOTO NUMBER
C YO= MIN.Y VALUE          YMAX= MAX Y VALUE
C  NY= NO. OF Y SLICES USED NFR= NO. OF FRINGES NSMTH= NO. OF
C  POINTS TO BE AVERAGED IN SMOOTHING
C NY=NO. OF EVENLY SPACED YSLICES (Y IS ALONG FRINGE)
C  NFR=NO OF FRINGES MAX.125 (MAX NO OF Y =150 -BOTH LIMITED
C BY THE DIMENSION STATEMENTS)
```

```
C D= FRINGE SEP. ON PHOTO   FRACT= ACTUAL FRINGE SEP. AT JET
C ERROR= TOLERANCE ON FRINGE SHIFT IN RADIANS  SIGN= + OR - 1.
      DELY = (YMAX - YO) / FLOAT(NY)
      YOO = YO
C
      DO 80 IFRNO = 1, NFR
C SET UP ARRAYS FOR ONE FRINGE (FRINGE NO=IFRNO)
        READ (5,200) IF, N
        READ (5,210) (IZ(I),IY(I),I=1,N)
C  N=1 IMPLIES A STRAIGHT FRINGE
        IF (N .NE. 1) GO TO 10
        N = 3
        IY(1) = IFIX(YMAX*1000.)
        IY(2) = IFIX((YMAX + YOO)/2.*1000.)
        IY(3) = IFIX(YOO*1000.)
        IZ(2) = IZ(1)
        IZ(3) = IZ(1)
C FIRST SEE IF IY IS IN DESCENDING OR ASCENDING ORDER
   10   IF (IY(2) - IY(1)) 20, 20, 40
C DESCENDING ORDER
   20   DO 30 JJ = 1, N
          Z(JJ) = FLOAT(IZ(JJ)) / 1000.
          Y(JJ) = FLOAT(IY(JJ)) / 1000.
   30   CONTINUE
        GO TO 60
C ASCENDING ORDER
   40   DO 50 JJ = 1, N
          Z(N - JJ + 1) = FLOAT(IZ(JJ)) / 1000.
          Y(N - JJ + 1) = FLOAT(IY(JJ)) / 1000.
   50   CONTINUE
   60   CONTINUE
C CALCULATE THE RAW DATA
C SLICE Y=1 MUST CROSS UNDEVIATED FRINGES (ALSO Y=NY)
C RAW(A,B)=Z DIST. FROM Z ORIGIN FOR FRINGE B ON LINE A
C DO SPLINE INTERPOLATION
        CALL SPLINA(Y, Z, N)
        YO = YOO
        DO 70 J = 1, NY
          CALL TERPA(YO, OUT)
          RAW(J,IFRNO) = OUT
          YO = YO + DELY
   70   CONTINUE
   80 CONTINUE
      DO 90 I = 1, NY
   90 WRITE (6,220) (RAW(I,J),J=1,NFR)
      RETURN
  100 FORMAT (' ', '  ')
  110 FORMAT (I3)

  120 FORMAT (2F8.3)
  130 FORMAT (' ', ' YO=', F8.3, ' YMAX=', F8.3)
  140 FORMAT (3I3)
  150 FORMAT (' ', ' YSLICES =', I4, ' FRINGES =', I4,
     1        ' SMTH =', I4)
  160 FORMAT (2F8.3)
  170 FORMAT (' ', ' FRINGESPACEPHOTO=', F8.3,
```

```
     1       ' FRINGESPACEJET=', F8.3)
  180 FORMAT (2F8.4)
  190 FORMAT (' ', ' ERROR RADIANS=', F8.4, ' SIGN USED', F8.4)
  200 FORMAT (I6, I5)
  210 FORMAT (6(1X,2I6))
  220 FORMAT (' ', (14F7.3))
  230 FORMAT (' ', ' PHOTO # ', I5)
      END
C=============================================================
      SUBROUTINE DLACT(RAW, DELACT, NY, NFR, D)
C CALCULATE THE ACTUAL PHASE SHIFT(ON A FRINGE)
      DIMENSION RAW(150,125), DELACT(150,125)
      DO 20 IY = 1, NY
        DO 10 IFRNO = 1, NFR
C USE AVERAGE OF END POINTS AS POSITION OF UNDEVIATED FRINGE
          DLAVE = (RAW(1,IFRNO) + RAW(NY,IFRNO)) / 2.
C  D=FRINGE SPACING ON SOURCE
          DELACT(IY,IFRNO) = (RAW(IY,IFRNO) - DLAVE) * 6.28 / D
   10   CONTINUE
        WRITE (6,30) (DELACT(IY,J),J=1,NFR)
   20 CONTINUE
      RETURN
   30 FORMAT (' ', 20F6.2)
      END
C=============================================================
      SUBROUTINE DLINT(RAW, DELACT, DELINT, NY, NFR, ERROR,
     1           D, SIGN, NSMTH)
      DIMENSION RAW(150,125), DELACT(150,125), DELINT(150,125)
      DIMENSION Z(125), DEL(125), Y(10000)
C SPLINE INTERPOLATION USED
C CALCULATE THE PHASE SHIFT ALONG LINE OF UNDEVIATED FRINGE
      NFRMAX = NFR - 1
      DO 90 IY = 1, NY
C FIRST SEE IF Z IS IN DESCENDING OR ASCENDING ORDER
        IF (RAW(1,2) - RAW(1,1)) 10, 10, 30
C DESCENDING ORDER
   10   DO 20 IFRNO = 1, NFRMAX
          Z(IFRNO) = RAW(IY,IFRNO)
          DEL(IFRNO) = DELACT(IY,IFRNO)
   20   CONTINUE
        GO TO 50
C ASCENDING ORDER
   30   DO 40 IFRNO = 1, NFRMAX
          Z(NFRMAX - IFRNO + 1) = RAW(IY,IFRNO)
          DEL(NFRMAX - IFRNO + 1) = DELACT(IY,IFRNO)
   40   CONTINUE
   50   CONTINUE
C DO THE ACTUAL INTERPOLATION
        CALL SPLINA(Z, DEL, NFRMAX)
        DO 60 IFRNO = 1, NFRMAX
C USE AVERAGE OF END  POINTS AS POSITION OF UNDEVIATED FRINGE
          ZO = (RAW(1,IFRNO) + RAW(NY,IFRNO)) / 2.
          CALL TERPA(ZO, OUT)
          DELINT(IY,IFRNO) = OUT
          IF (OUT*SIGN .LT. 0 .OR. ABS(OUT) .LT. ERROR)
     1     DELINT(IY,IFRNO) = 0.0
```

```
C DUE TO ERRORS IN DIGITIZING,SMALL PHASE SHIFTS ARE MADE ZERO
C ALSO IF FRINGE GOES 'WRONG' WAY PHASE SHIFT IS MADE ZERO
   60    CONTINUE
C SMOOTH THE DATA
         DO 70 KKK = 1, NFRMAX
           Y(KKK) = DELINT(IY,KKK)
   70    CONTINUE
         CALL GSMTH(Y, NSMTH, NFRMAX)
         DO 80 KKK = 1, NFRMAX
           DELINT(IY,KKK) = Y(KKK)
   80    CONTINUE
         WRITE (6,110) (DELINT(IY,J),J=1,NFRMAX)
   90 CONTINUE
  100 RETURN
  110 FORMAT (' ', 20F6.2)
      END
C=============================================================
      SUBROUTINE ABDATA(DELINT, NY, NFR, DELRAD, IRADS, FLAG,
     1            SIGN, ERROR)
C PREPARE DATA FOR ABEL INVERSION PROGRAM
      LOGICAL FLAG(1000)
      DIMENSION ICNTR(1000), IRADS(1000), DELRAD(150,125),
     1          DELINT(150,125)
C CALCULATE CENTRE OF FRINGE PATTERN
C CENTRE =SUM(IY*DELINT(IY,IFRNO))/SUM(DELINT(IY,IFRNO)
      NFRMAX = NFR - 1
      DO 30 IFRNO = 1, NFRMAX
        SUM1 = 0
        SUM2 = 0
        DO 10 IY = 1, NY
          SUM1 = SUM1 + FLOAT(IY) * DELINT(IY,IFRNO)
          SUM2 = SUM2 + DELINT(IY,IFRNO)
   10   CONTINUE
C IF TOTAL AMT. FRINGE SHIFT TOO SMALL REPORT NO FRINGE SHIFT
        IF (ABS(SUM2) .LT. ERROR) GO TO 20
        ICNTR(IFRNO) = (SUM1/SUM2) + .5
        WRITE (6,110) IFRNO, ICNTR(IFRNO)
        GO TO 30
   20   FLAG(IFRNO) = .FALSE.
        WRITE (6,100) IFRNO
   30 CONTINUE
C NOW CALCULATE RADIUS OF FRINGE PATTERN
C RADIUS = MIN. DIST. FROM CENTRE WHERE DEL=0 ON BOTH SIDES
      DO 70 IFRNO = 1, NFRMAX
        IF ( .NOT. FLAG(IFRNO)) GO TO 70
        DO 40 I = 1, NY
          IP = ICNTR(IFRNO) + I
          IM = ICNTR(IFRNO) - I
C IF CANNOT FIND ZERO FRINGE SHIFT ON ENDS REPORT ERROR
          IF (IP .GT. NY .OR. IM .LT. 1) GO TO 60
          IF (ABS(DELINT(IP,IFRNO)) .LT. ERROR .AND.
     1       ABS(DELINT(IM,IFRNO)) .LT. ERROR) GO TO 50
   40   CONTINUE
   50   WRITE (6,130) IFRNO, I
        IRADS(IFRNO) = I
        IF (IRADS(IFRNO) .GT. 2) GO TO 70
```

```
   60   WRITE (6,120) IFRNO
        FLAG(IFRNO) = .FALSE.
   70 CONTINUE
C CALCULATE DEL AS A FUNCTION OF RADIUS
C DELRAD=  AVERAGE OF DEL AT PLUS/MINUS EQUAL DIST. FROM CENTRE
      DO 90 IFRNO = 1, NFRMAX
        IF ( .NOT. FLAG(IFRNO)) GO TO 90
        JMAX = IRADS(IFRNO) + 1
        DO 80 J = 1, JMAX
          JDIF = JMAX - J
          JP = ICNTR(IFRNO) + JDIF
          JM = ICNTR(IFRNO) - JDIF
          DELRAD(J,IFRNO) = (DELINT(JP,IFRNO) + DELINT(JM,IFRNO))
     1     SIGN
C SIGN HERE BECAUSE OF WAY FRINGE SHIFT CALCULATED
   80   CONTINUE
   90 CONTINUE
      RETURN
  100 FORMAT (' ', ' NO SHIFT FRINGE NO', I4)
  110 FORMAT (' ', '  CENTRE OF FRINGE', I5, '  IS', I5)
  120 FORMAT (' ', ' FRINGE NO', I4, ' IS TOO SKEWED/TOO LARGE /T
     1L')
  130 FORMAT (' ', ' FRINGE NO', I4, ' HAS RADIUS', I4)
      END
C=============================================================
C               C P C   PROGRAM   A B S C
C               ABEL INVERSION  - DIRECT
C=============================================================
C WRITTEN BY L.S. FAN AND W. SQUIRE.
C REF:  COMP. PHYS. COMMUN. 10 (1975) 98
C     XLO=CONSTANT LIMIT OF INTEGRAL
C     NA=NUMBER OF DATA POINTS ( WHICH DO
C     NOT HAVE TO BE EQUALLY SPACED)
C     NP=NUMBER OF DIVISIONS FOR INTEGRATION,
C     (LIMITED TO 300 BY DIMENSION STATEMENT)
C     NSS=NUMBER OF STEPS OMITTED NEAR SINGULARITY
C     NOUT=NUMBER OF OUTPUT POINTS
C     X=ARRAY WITH INDEPENDENT VARIABLE IN
C     DESCENDING ORDER
C     Y=ARRAY WITH CORRESPONDing VALUES OF DEPENDENT VARIABLE
C=============================================================
      SUBROUTINE ABEL(DELRAD, NDS, IFRNO, ROUT, DENS, NOUT, D,
     1           DELY, FRACT)
C     PROGRAM FOR SOLVING ABEL'S
C     EQUATION USING TABULATE DATA
      DIMENSION U(300), T(300), X(300), Y(300), DELRAD(150,125),
     1          IRADS(1000)
      DIMENSION ROUT(1000), DENS(1000)
C CREATE DATA ARRAYS
      YSCALE = DELY * FRACT / D
C YSCALE=DISTANCE 1 UNIT IS IN REAL UNITS (MM)
      DO 10 I = 1, NDS
        X(I) = (NDS - I) * YSCALE
        Y(I) = DELRAD(I,IFRNO)
   10 CONTINUE
C WRITE OUT DATA ARRAYS
```

```
      DO 20 I = 1, NDS
        WRITE (6,60) X(I), Y(I)
   20 CONTINUE
C SET UP SPECIFICATIONS FOR PROGRAM
      IOUT = 6
      XLO = (FLOAT(NDS) - 1) * YSCALE
      NP = 50
      NA = NDS
      NSS = 2
      NOUT = 21
      WLAMDA = 694.3E-06 / 2. / 3.1415926
C WLAMDA = WAVELENGTH OF PROBE LASER (RUBY) (MM)/2PI
      DSCALE = (10.6/.6943) ** 2
C DSCALE=NCRPROBE/NCRCO2
      WRITE (6,40) XLO, NA, NP, NSS, NOUT
      WRITE (IOUT,50)
C WRITE OUT HEADINGS FOR OUTPUT
      WRITE (IOUT,70)
C     INVERSION OF ABEL'S INTEGRAL EQUATION
C     SMOOTHING DATA AND INTERPOLATION BY CALLING SPLINA
C     SET UP INTERPOLATION OF INPUT DATA
      CALL SPLINA(X, Y, NA)
      H = -XLO / FLOAT(NP)
C     INVERT ABEL INTEGRAL BY CALLING VLIGM
      NP = NP - NSS
      CALL VLIGM(XLO, H, NP, U, T)
      U(1) = 0.0
      T(1) = XLO
C     INTERPOLATION AND EXTRAPOLATION FOR OUTPUT
      NS = NP + 1
      CALL SPLINA(T, U, NS)
      DO 30 I = 1, NOUT
        V = FLOAT(I - 1) / FLOAT(NOUT - 1) * XLO
        CALL TERPA(V, VV)
        VO = V
        VVO = VV * WLAMDA
        ROUT(I) = VO
        DENS(I) = VVO * 2. * DSCALE
C IF DENS TOO LARGE DO NOT USE APPROXIMATIONS
        IF (DENS(I) .GT. .1) DENS(I) = (1. - (1. - VVO)**2) *
     1   DSCALE
C  IF DENSITY .LT. ZERO, MAKE IT ZERO (WILL FOUL UP RAY TRACING
C OTHERWISE)
        IF (DENS(I) .LT. 0.0) DENS(I) = 0.0
        WRITE (IOUT,80) ROUT(I), DENS(I)
   30 CONTINUE
      RETURN
   40 FORMAT (' ', ' XLO=', F8.3, ' NA=', I4, ' NP=', I4,
     1       ' NSS=, I4, ' NOUT=', I4)
   50 FORMAT ('1')
   60 FORMAT (2F10.4)
   70 FORMAT (' ', 3X, 'RADIUS', 29X, 'N(CALCUL.)'/)
   80 FORMAT (G10.4, 26X, G10.4, 8X, G10.4)
      END
C=============================================================
      SUBROUTINE SPLINA(X, Y, N)
```

```
C      SUBROUTINE USING RAMAMOORTHY AND NARAYANA
C      SPLINE PROCEDURE FOR INTERPOLATION
C      SUBROUTINE HAS TWO ENTRIES SPLINA AND TERPA
C      ARGUMENTS FOR SPLINA ARE:
C      X=ARRAY WITH INDEPENDENT VARIABLE IN
C      DESCENDING ORDER
C      Y=ARRAY WITH CORRESPONDing VALUES OF DEPENDENT VARIABLE
C      N=NUMBER OF DATA POINTS
C      ARGUMENTS FOR TERPA ARE:
C      XV=VALUE OF INDEPENDENT VARIABLE
C      YV=LOCATION WHERE CORRESPoNDING VALUE OF DEPENDENT
C      VARIABLE IS PUT
       DIMENSION W(300), Q(300), B(300), A(300), C(300), S(300),
      1          Z(300)
       DIMENSION X(N), Y(N)
       DATA A(1), C(1) /-1., 0.0/
C CHECK TO SEE IF DATA POINTS ARE TOO CLOSE (MAYBE EQUAL)
       DO 10 J = 2, N
         W(J) = X(J) - X(J - 1)
         IF (ABS(W(J)) .LT. .005) WRITE (6,60) X(J)
    10 CONTINUE
       NM = N - 1
       DO 20 J = 2, NM
         WJ = W(J)
         WP = W(J + 1)
         WS = WJ + WP
         QJ = WJ / WS
         Q(J) = QJ
         QA = 1. - .5 * QJ * A(J - 1)
         A(J) = .5 * (1. - QJ) / QA
         B(J) = 3. * (WP*Y(J - 1) - WS*Y(J) + WJ*Y(J + 1)) / WP /
      1       WJ / WS
         C(J) = (B(J) - .5*QJ*C(J - 1)) / QA
    20 CONTINUE
       S(N) = C(NM) / (1. + A(NM))
       S(NM) = S(N)
       NMM = N - 2
       DO 30 JJ = 1, NMM
         J = NMM - JJ + 1
         S(J) = C(J) - A(J) * S(J + 1)
    30 CONTINUE
       RETURN
C=============================================================
       ENTRY TERPA(XV,YV)
C      INTERPOLATION PROCEDURE
       DO 40 JJ = 2, N
         J = JJ
         IF (XV .LT. X(J)) GO TO 40
         GO TO 50
    40 CONTINUE
    50 WJ = W(J)
       D1 = (XV - X(J - 1)) / WJ
       D2 = (X(J) - XV) / WJ
       D3 = WJ * WJ / 6.
       YV = D1 * (Y(J) + D3*(D1*D1 - 1.)*S(J))
       YV = YV + D2 * (Y(J - 1) + D3*(D2*D2 - 1.)*S(J - 1))
```

```
      RETURN
   60 FORMAT (' ', G12.5, '  CHECK:TWO POINTS VERY CLOSE  ')
      END
C=======================================================
      SUBROUTINE VLIGM(XLO, H, NP, U, T)
C     SUBROUTINE FOR SOLVING LINEAR VOLTERRA INTEGRAL
C     EQUATION OF THE FIRST KIND USING THE GENERALIZED
C     MIDPOINT RULE WITH THE KERNEL AS WEIGHT FUNCTION
C     XLO=LOWER LIMIT OF INTEGRAL
C     H=STEP SIZE
C     NP=NUMBER OF STEPS
C     KERNEL WITH RESPECT TO T
C     U=SINGLY SUBSCRIPTED ARRAY FOR SOLUTION
C     T=SINGLY SUBSCRIPTED ARRAY FOR INDEPENDENT VARIABLE
      DIMENSION U(1), T(1)
      HXT(X,TM) = -2. * SQRT(TM*TM - X*X)
      S = 0.5 * H
      X = XLO + H
      T(2) = X - S
      HLO = HXT(X,XLO)
      HUP = HXT(X,X)
      CALL TERPA(X, FXX)
      U(2) = FXX / (HUP - HLO)
      DO 20 I = 2, NP
        X = H * FLOAT(I) + XLO
        CALL TERPA(X, FXX)
        T(I + 1) = X - S
        SUM = 0.0
        HUP = HXT(X,XLO)
        NM = I - 1
        DO 10 J = 1, NM
          HLO = HUP
          HUP = HXT(X,T(J + 1) + S)
   10   SUM = SUM + U(J + 1) * (HUP - HLO)
        U(I + 1) = (FXX - SUM) / (HXT(X,X) - HUP)
   20 CONTINUE
      RETURN
      END
C=======================================================
      SUBROUTINE GSMTH(Y, N, NP)
C DOES GENERAL SMOOTHING USING 2N+1 POINT AVERAGING
      DIMENSION Y(10000), WY(10000)
      DO 30 I = 1, NP
        SUM = Y(I)
        NU = MIN0(I - 1,NP - I,N)
        IF (NU .EQ. 0) GO TO 20
        DO 10 J = 1, NU
          SUM = SUM + Y(I - J) + Y(I + J)
   10   CONTINUE
   20   WY(I) = SUM / (2.*FLOAT(NU) + 1.)
   30 CONTINUE
      DO 40 K = 1, NP
        Y(K) = WY(K)
   40 CONTINUE
      RETURN
      END
```

APPENDIX 2 RAMAN ENERGY CALCULATIONS

The calculations to follow will show the density regions where SRS can occur and what are the phase velocities that can occur .

Wave Matching (1) $\omega_o=\omega_s+\omega_K$

(2) $k_o=k_s+k$

Dispersion Relations (3) $\omega_K^2=\omega_p^2+3\kappa Tk^2/m$

(4) $\omega_s^2=\omega_p^2+c^2k_s^2$

(5) $\omega_o^2=\omega_p^2+c^2k_o^2$

(1) and (2) into (4) yields

6(a) $(\omega_o-\omega_K)**2=\omega_p^2+c^2(k_o-k)**2$

Expanding and (5) to eliminate ω_o^2

6(b) $\omega_K^2-2\omega_o\omega_K=c^2(k^2-2kk_o)=c^2k_o^2(\xi^2-2\xi)$ $(k=\xi k_o)$

Eliminate $c^2k_o^2$ by (5)

(7) $\omega_K^2-2\omega_o\omega_K=(\omega_o^2-\omega_p^2)(\xi^2-2\xi)$

Replace ω_K^2 by (3) and divide by ω_p^2

(8) $1+3\kappa T\xi^2(\omega_o^2/\omega_p^2-1)/(mc^2)-2\omega_o/\omega_p\sqrt{(1+3\kappa T\xi^2(\omega_o^2/\omega_p^2-1)/(mc^2))}$
$=(\omega_o^2/\omega_p^2-1)(\xi^2-2\xi)$

Rearrange and call $\omega_o/\omega_p=\sqrt{(n_{CR}/n)}=a$

(9) $\xi^2-2\xi+(2a\sqrt{(1+3\kappa T\xi^2(a^2-1)/(mc^2))}-1-3\kappa T\xi^2(a^2-1)/(mc^2))/(a^2-1)=0$

Let T=0

(10) $\xi^2-2\xi+(2a-1)/(a^2-1)=0$

This quadratic has real roots if $a>2$ or $n<n_{CR}/4$.

The phase velocity is easily calculated.

(11) $v_{PH}/c=\sqrt{(\omega_p^2+3\kappa Tk^2/m)}/(kc)$

(12) $v_{PH}/c=\sqrt{(\omega_p^2/k^2/c^2+3\kappa T/(mc^2))}$

Letting $k=\xi k_o$ and eliminating $k_o^2c^2$ by (5)

(13) $v_{pH}/c=\sqrt{(\omega_p^2/(\xi^2(\omega_o^2-\omega_p^2))+3\kappa T/(mc^2))}$.

Finally we get

(14) $v_{pH}/c=\sqrt{(1/(\xi^2(a^2-1))+3\kappa T/(mc^2))}$

Again let $T=0$

(15) $mv_{pH}^2/2=mc^2/2/(\xi^2(a^2-1))$.

This is the expression that was plotted.

REFERENCES

Baldis,H.A.,Walsh,C.J. Phys. Fluids 26,1364 (1983)

Berger,R.G.,Brooks,R.D.,Pietrzyk,Z.A. Phys. Fluids 26,353 (1983)

Bernard,J.E. Ph.D Thesis 1984 (University of British Columbia)

Born,M.,Wolf,E. Principles of Optics (6 th. Ed.) Pergammon Press

Burak,I.,Steinfeld,J.I.,Sutton,D.G. J.Quant.Spectrosc. And Radiat.Trans. 9,959(1969)

Chen,F.F. Physical Mechanisms for Laser Plasma Parametric Instabilities in Laser Plasmas and Nuclear Energy ed. Hora,H. Plenum Press New York (1975)

Chen,F.F Introduction to Plasma Physics Plenum Press New York (1974)

Chen,H.H.,Liu,C.S. Phys. Rev. Lett. 39,1147 (1977)

Chorlton,F. Textbook of Fluid Dynamics Van Nostrand London (1967)

Cohen,B.I.,Max,C.E. Phys. Fluids 22,1115 (1979)

Dubois,D.F. Laser Induced Instabilities and Anomalous Absorption in Dense Plasmas in Laser Interaction and Related Plasma Phenomena v.3a ed. Schwarz,H.J.,Hora,H. Plenum Press,New York (1974) p.267-289

Dyson,N.A. Xrays in Atomic and Nuclear Physics Longman ,London,(1973)

Ebrahim,N.A.,Joshi,C.,Baldis,H.A. Phys. Lett. 84A,253 (1981)

Estabrook,K.,Kruer,W.L.,Lasinski,B.F. Phys.Rev.Lett. 45,1399 (1980)

Estabrook,K.,Kruer,W.L. Phys.Rev.Lett 40,42(1978)

Estabrook,K. Phys.Rev.Lett 47,1396(1981)

Estabrook,K.,Kruer,W.L. Phys. Fluids 26,1982 (1983)

Fan,L.S.,Squire,W. Comp.Phys.Comm. 10,98 (1975)

Forslund,D.W.,Kindel,J.M. ,Lee,K. Phys.Rev.Lett. 39,284 (1977)

Forslund,D.W., Kindel,J.M., Lindman,E.L. Phys. Fluids 18,1002 (1975)

Giles,R. Ph.D. Thesis 1983 (University of Alberta)

Herbst,M.J., Stamper,J.A. ,Whitlak,R.R., Lehmberg,R.H., Ripin,B.H. Phys.Rev.Lett 46,328 (1981)

Hiob,E.,Barnard,A,J, Phys. Fluids 26,3119 (1983)

Houtman,H.,Walsh,C.J. UBC Plasma Physics Internal Report No.79

Ichimaru,S. Basic Principles of Plasma Physics ,Benjamin

Cummings Pub.Co.,Reading Mass.,(1973)

Jackson,E.A. Phys. Rev. 153,255 (1967)

Jorna,S. Phys. Fluids 17,765 (1974)

Joshi,C., Tajima,T., Dawson,J.M., Baldis,H.A., Ebrahim,N.A. Phys. Rev. Lett. 47,1285 (1981)

Karttunen,S.J., Plasma Phys. 22,151 (1980)

Karttunnen,.S.J.,Salomaa,R.R.E. Plasma Phys. 22,247 (1979)

Kolodner,P.,Yablonovitch,E. Phys.Rev.Lett 37,1754 (1976)

Kruer,W.L. Comments Plasma Phys. Cont. Fusion 6,167(1981)

Kruer,W.L., Valeo,E.J., Estabrook,K. Phys. Rev. Lett. 32,1172 (1975)

Langdon,B.,Lasinski,B. Electromagnetic and Relativistic Plasma Simulation Models in Methods in Computational Physics , ed. Alder,B.; Fernbach,S.; Rotenberg,M. Academic Press New York (1976)

Langdon,B.,Lasinski,B. Laser Program Annual Report 1977 Lawrence Livermore Report No UCRL-50021-77 (1978) p.4-49

Lee,Y.C.,Kaw,P.K. Phys.Rev.Lett. 32,135 (1974)

Liu,C.S. ,Rosenbluth,M.N. Phys.Rev.Lett 29,565(1972)

Livingood,J.J. Optics of Dipole Magnets Academic Press New

York (1969)

Meyer,J., Bernard,J.E., Hilko,B., Houtman,H., McIntosh,G., Popil,R. Proceedings of the XVI International Conference on Phenomena in Ionized Gases V2 ed. Botticher,W., Wenk,H., Schulz-Gulde,E. (1983)

Meyerott,A.J.,Fisher,P.C. ,Roethig,D.T. Rev.Sci.Instr. 35,669 (1964)

Ng,A., Salzmann,D., Offenberger,A.A. Phys.Rev.Lett 43,1502 (1979)

Popil,R. ,Meyer,J. J.Appl. Phys. 52,5846 (1981)

Popil,R. Ph.D. Thesis 1984 (University of British Columbia)

Prescott,J.R., Rupaal,A.S. Can.J.Phys. 39,221 (1961)

Rosenbluth,M.N. Phys.Rev.Lett 29,565(1972)

Segre,E. Nuclei and Particles 2nd ed. Benjamin Cummings Reading,Mass. (1977)

Shapiro,A.H. Dynamics and Thermodynamics of Compressible Fluid Flow V.1 Ronald Press Co. New York (1953)

Silin,V.P., Tikhonchuk,V.T. Soviet Phys. JETP 54,1075 (1982)

Simon,A., Short,R.W., Williams,E.W.., Dewardre,T. ,private communication

Spitzer,L. Physics of Fully Ionized Gases 2nd. Ed. Interscience Pub.,New York (1962)

Von Schmeling,H. Zeit. Phys. 160,520 (1960)